J. Fluid Mech. (1977), *vol.* 83, *part* 3, *pp.* 433–464
Printed in Great Britain

Wall shear stress caused by small amplitude perturbations of turbulent boundary-layer flow: an experimental investigation

By D. RONNEBERGER AND C. D. AHRENS
Drittes Physikalisches Institut, Universität Göttingen, Germany

(Received 5 January 1977)

The oscillation of the wall shear stress caused by imposing sound on a turbulent boundary-layer flow constitutes a boundary condition for the solution of the acoustic wave equation. The no-slip condition at the wall requires the excitation of a shear wave which is superimposed on the sound wave. The shear wave propagates into the turbulent medium. The wall impedance (shear stress/velocity) of streamwise polarized shear waves has been measured in two different ways, namely (*a*) by evaluating the phase velocity and the attenuation of a plane sound wave which propagates in turbulent pipe flow, and (*b*) by evaluating the resonance frequency and the quality factor of a longitudinally vibrating glass pipe which carries turbulent flow. The results, which were obtained over a wide range of Strouhal numbers, exhibit very good agreement between the two measuring methods. The wall shear stress impedance is strongly affected by the turbulence. This indicates that the turbulent shear stress is modulated by the shear wave. At all measuring conditions, the propagation of the shear wave was confined essentially to the inner portion of the turbulent boundary layer. In principle, two different Strouhal numbers, based on inner and outer variables respectively, describe the dynamics of the Reynolds stress, even in the inner layer (Laufer & Badri Narayanan 1971). However, it turns out that the outer Strouhal number (based on the diameter and the centre-line velocity) has no noticeable effect on the wall shear stress impedance. The dependence of the impedance on the inner Strouhal number (based on the friction velocity and the viscosity) reveals that the shear wave is strongly reflected at the edge of the viscous sublayer. It is concluded that the stress-to-strain ratio at the edge of the viscous sublayer corresponds either to a viscoelastic medium or even to a medium with negative viscosity.

1. Introduction

Unsteady turbulent flows have been investigated mostly with large perturbations of the mean flow, which, in some cases, was even non-existent (see, for example, Eichelbrenner 1971; Brocher 1977). Only in recent years have several papers on small amplitude perturbations of turbulent flows been published (Kendall 1970; Hussain & Reynolds 1970*a*, 1972; Reynolds & Hussain 1972; Davis 1972, 1974; Ahrens 1973; Norris & Reynolds 1975; Acharya & Reynolds 1975; Ronneberger 1975). The experimental investigations in this field were essentially stimulated by Landahl's (1967) suggestion that the turbulence in shear layers might be composed of waves (Hussain & Reynolds 1970*b*). Additional interest stems from the study of turbulent flow over

waving boundaries (Kendall 1970; Stewart 1970; Norris & Reynolds 1975). Furthermore, the exploration of a turbulent flow responding to small variations in the boundary or initial conditions has the advantage of experimental and theoretical simplicity, which is achieved by the linearization of the governing equations.

A mathematical description of a turbulent flow containing coherent perturbations is usually attained by decomposition of the field quantities into three parts (see, for example, Hussain & Reynolds 1970*b*);

$$f = \bar{f} + \tilde{f} + f',$$

which denote the time average of the quantity, the fluctuation caused by the coherent perturbation and the turbulent fluctuation, respectively. In the case of periodic perturbations, $\tilde{f}$ may be extracted from the total quantity f by 'phase averaging' and subtraction of the mean part $\bar{f}$. This corresponds, in the case of small amplitude perturbations, to the determination of the frequency response of a very noisy system, the input and the output of which are the external perturbation and the quantity f, respectively. Standard techniques are available for the experimental accomplishment of this task. The response to small disturbances of the equilibrium state is a well established method to describe the dynamics of a physical system, and the common relaxation methods have to be quoted in this context.

A central problem in turbulence research is the determination of the turbulent stresses as a function of the mean flow field. Because of the well-known closure problem preventing the calculation of correlations between turbulently fluctuating quantities on the basis of the Navier–Stokes equations, it is not possible to predict the Reynolds stresses except by semi-empirical relations between the variables of the flow field. Many, more or less sophisticated, closure models have been developed which yield excellent results for various cases of steady turbulent flow. However, where these models have been applied to unsteady flows, the agreement between the predicted and experimental data has been poor in most cases. In order to find reasons for the failure of these turbulence models more measurements of the perturbation stresses are needed.

The initiative for the present investigation was provided by a study of sound propagation in turbulent pipe flow. The attenuation of a plane sound wave propagating through a pipe had been found to increase strongly compared with that for the medium at rest if the Strouhal number (based on the wall parameters of the boundary layer) was decreased below a critical value (Ahrens & Ronneberger 1971). The sound attenuation is caused by the diffusion of momentum and heat: the boundary conditions at the pipe wall (no slip, and no oscillation of the temperature) require that the sound wave excites a shear wave propagated by viscous and turbulent shear stresses and a heat conduction wave at the wall. In the case of low Mach number flow, the effect of these diffusion waves on the sound propagation is described by the complex 'wall impedances' of these waves, i.e. by the ratio of the complex amplitudes of the shear stress and the velocity in the shear wave and the ratio of the conducted heat and the temperature in the heat conduction wave, the ratios being evaluated at the wall. The real parts of these impedances correspond to the loss of acoustic energy, so the real parts determine the attenuation of the sound wave whereas the imaginary parts of the impedances cause a change in the phase velocity. The diffusion of momentum and of heat is strongly influenced by turbulent convection. Thus both impedances – the

wall shear stress impedance $z_\tau = \tilde{\tau}_w/\tilde{u}_w$ and the wall heat conduction impedance $z_q = \tilde{q}_w/\tilde{T}_w$ – are affected by the turbulent transport of momentum and of heat.

Our experimental investigation is concerned with the wall impedance of shear waves which are polarized in the mean-flow direction and propagate in the direction normal to the wall. One can excite these waves either by small perturbations of the mean-flow velocity (sound) or by longitudinal oscillations of the pipe wall. Both methods have been used.

A general view of the propagation of a shear wave in the turbulent medium is obtained if one realizes that the ratio of shear stress to strain is a strongly varying complex function of the distance from the wall. Thus the shear wave propagates in an inhomogeneous medium and may be reflected. The reflected wave influences the wall shear stress impedance and thus information on the stress-to-strain ratio in the turbulence may be obtained from measurements of the impedance.

In the viscous sublayer the shear stress and the strain rate are related by the molecular viscosity. Thus one can easily calculate the propagation of the shear wave in the sublayer. The amplitude of the wave decays by a factor of e within the distance $\delta_A = (2\nu/\omega)^{\frac{1}{2}}$, which is known as the thickness of the Stokes layer in laminar oscillating flow or the acoustical boundary-layer thickness. Because of this rapid decay, the shear wave passes through the sublayer only at large values of the parameter

$$\delta_A^+ = \delta_A u_\tau/\nu = \left(\frac{2u_\tau^2}{\nu\omega}\right)^{\frac{1}{2}} \tag{1}$$

($u_\tau = (\bar{\tau}_w/\rho)^{\frac{1}{2}}$ = friction velocity, $\bar{\tau}_w$ = mean wall shear stress, ρ = density, ν = kinematic viscosity, ω = angular frequency of the shear wave and a superscript + denotes a quantity non-dimensionalized by ν and u_τ). The limited penetration depth of the shear wave implies that the wall shear stress impedance can be influenced by the turbulence only if $\delta_A^+ \gg 1$. The second part of (1) demonstrates that δ_A^+ is closely related to the Strouhal number $\omega\nu/u_\tau^2$. If one assumes that the turbulent momentum transport in the inner portion of the boundary layer depends only on this Strouhal number, at least at large values of the Reynolds number based on the diameter of the pipe, the wall shear stress should be independent of the Reynolds number. In § 4.3 this question is discussed in detail. In fact, the dependence on the Reynolds number, if any, is rather small, so the normalized wall shear stress impedance $Z_\tau = z_\tau\,(\frac{1}{2}\omega\rho\mu)^{-\frac{1}{2}}$ depends mainly on δ_A^+, which is used as Strouhal parameter here.

It is clear from these considerations that the wall shear stress impedance is a function of just the Reynolds stresses which determine the propagation of coherent shear waves in the transition region of the turbulent boundary layer, and additional measurements similar to the experiment of Acharya & Reynolds (1975) are necessary to obtain definite values of these stresses. Nevertheless, the objective of the present investigation was not only the prediction of the sound propagation in low Mach number turbulent pipe flow, but also the collection of information on the dynamic properties of the turbulence at the edge of the viscous sublayer. Thus, in a preliminary experiment, the wall shear stress impedance was measured also in a drag-reducing flow of an aqueous 20 p.p.m. Separan solution.

2. Determination of the wall shear stress impedance from the complex wavenumber of sound in turbulent air flow through pipes

The experiment aimed at the evaluation of the wall shear stress impedance z_τ from the sound propagation in turbulent pipe flow is described by Ronneberger (1975). Therefore only a summary is presented here.

2.1. *Relation between the wall shear stress impedance and the sound wavenumber*

The complex wavenumber k of a plane sound wave in low Mach number pipe flow can be calculated from the equations of conservation of momentum, matter and energy by averaging these equations over the cross-section. If the diffusion of momentum and of heat is confined to a thin layer at the wall and if the wavelength is large compared with the pipe diameter, one obtains

$$\lim_{M\to 0} k = \frac{\omega}{c} - \frac{i}{r_i}\frac{z_\tau + (\gamma-1)\,c_p^{-1} z_q}{\rho c}, \quad \delta_A, \delta_A/Pr^{\frac{1}{2}} \ll r_i \tag{2}$$

(c = adiabatic sound speed, c_p = specific heat at constant pressure, γ = ratio of the specific heats, M = Mach number and r_i = inner radius of the pipe). δ_A^+ and eventually the Reynolds number have to be kept constant when taking the limit $M \to 0$. $\delta_A^+ \ll r_i^+$ is automatically satisfied in the case of large Reynolds numbers. The Prandtl number Pr is of the order of unity in gases. z_τ can be evaluated from the sound wavenumber according to (2) if z_q is known, and z_q can be computed if the turbulent heat transport in the heat conduction wave is known. Here we assume that the heat transport can be described by an effective diffusion constant and that this heat conductivity is independent of the frequency at the low Strouhal numbers at which the heat conduction wave penetrates the viscous sublayer; i.e. we calculate the propagation and the wall impedance of the heat conduction wave from turbulent heat transport data measured in steady flow by Ludwieg (1956). Figure 1 shows the normalized wall heat conduction impedance as a function of δ_A^+ in air, according to Ronneberger (1975). The calculation of $Z_q = z_q(\frac{1}{2}\omega\rho\lambda c_p)^{-\frac{1}{2}}$ was similar to that of Z_τ, which is described in § 4.2 (λ = molecular heat conductivity). The coefficient of turbulent heat conductivity near the wall was assumed to be $1{\cdot}08\rho c_p l_m^2 |d\bar{u}/dy|$ (l_m = mixing length), according to the findings of Ludwieg (1956). Cebeci (1973) recommends a value of the eddy conductivity which depends on the distance from the wall as well as on the Reynolds number and on the Prandtl number, but for the case of our experiments his estimation is almost identical to the value adopted here.

2.2. *Measurement of the attenuation and of the phase velocity of plane sound waves in pipes*

Principle. The second term on the right-hand side of (2) is of order of magnitude $10^{-1}\,\mathrm{m}^{-1}$. As an accuracy of 1 % was required, in a pipe about 1 m long, the ratios of sound pressures had to be determined with an accuracy of about 10^{-3}. It is not reasonable, under these conditions, to use a movable probe microphone (at 1 kHz, for example, the complex amplitude of the sound pressure is changed by 10^{-3}, on the average, if

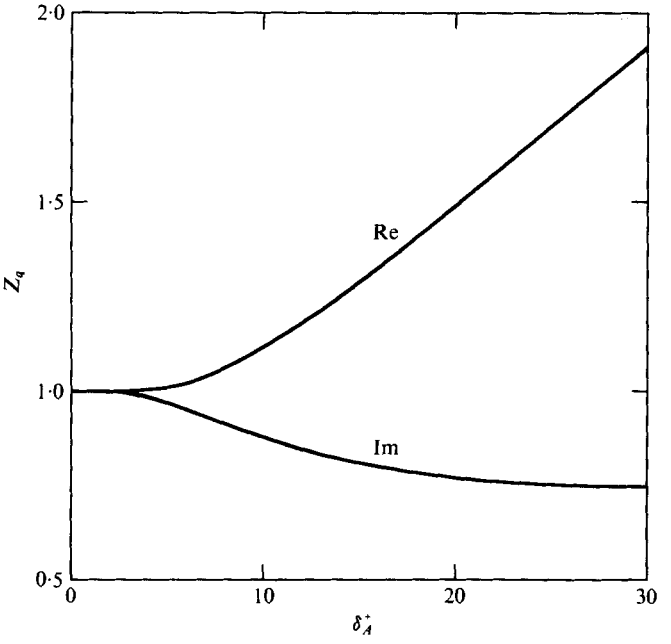

FIGURE 1. Normalized wall impedance of the heat conduction wave in air as a function of δ_A^+ (theoretical).

the probe is shifted by only 0·05 mm). Therefore ten microphones were built in the wall of the pipe at various axial positions. At each end of the pipe a loudspeaker can radiate into the pipe (see figure 3). So two different sound fields are generated. The output voltage of the νth microphone is given by

$$U_{\nu\kappa}(t) = \mathrm{Re}\,(\hat{U}_{\nu\kappa}\, e^{i\omega t}) = \mathrm{Re}\,(\sigma_\nu \tilde{p}_{\nu\kappa}\, e^{i\omega t}), \quad \kappa = 1, 2, \quad \nu = 1, 2, \ldots, 10. \tag{3}$$

$\tilde{p}_{\nu\kappa}$ are the complex amplitudes of the sound pressures at the νth microphone and σ_ν is the complex sensitivity. The ten ratios $\hat{U}_{\nu 1}/\hat{U}_{\nu 2}$ are independent of the σ_ν and are equal to $\tilde{p}_{\nu 1}/\tilde{p}_{\nu 2}$. Proceeding on the assumption that each of the sound fields consists of an incident wave and a reflected wave, one obtains the model equation for the sound pressure ratios at the ten microphones as

$$\frac{\tilde{p}_{\nu 1}}{\tilde{p}_{\nu 2}} = A\,\frac{1 + r_2 \exp(2i\bar{k}x_\nu)}{r_1 + \exp(2i\bar{k}x_\nu)}. \tag{4}$$

Hence one can determine the wavenumber $\bar{k}$ and the three other unknown parameters A, r_1 and r_2 by a regression analysis (A is proportional to the ratio of the two loudspeaker voltages while r_1 and r_2 are the acoustic reflexion coefficients at either end of the measuring pipe). $\bar{k}$ is the average of the wavenumbers for upstream and downstream propagation. However, in the model equation actually used, one has to include the gradient of $\bar{k}$ due to the pressure gradient in the pipe as well as the scattering of the sound waves by the microphones.

It is sufficient to determine only the average of the two wavenumbers since only the wavenumbers extrapolated to $M = 0$ are used for the calculation of the wall shear stress impedance according to (2). It is possible, however, to evaluate also the difference

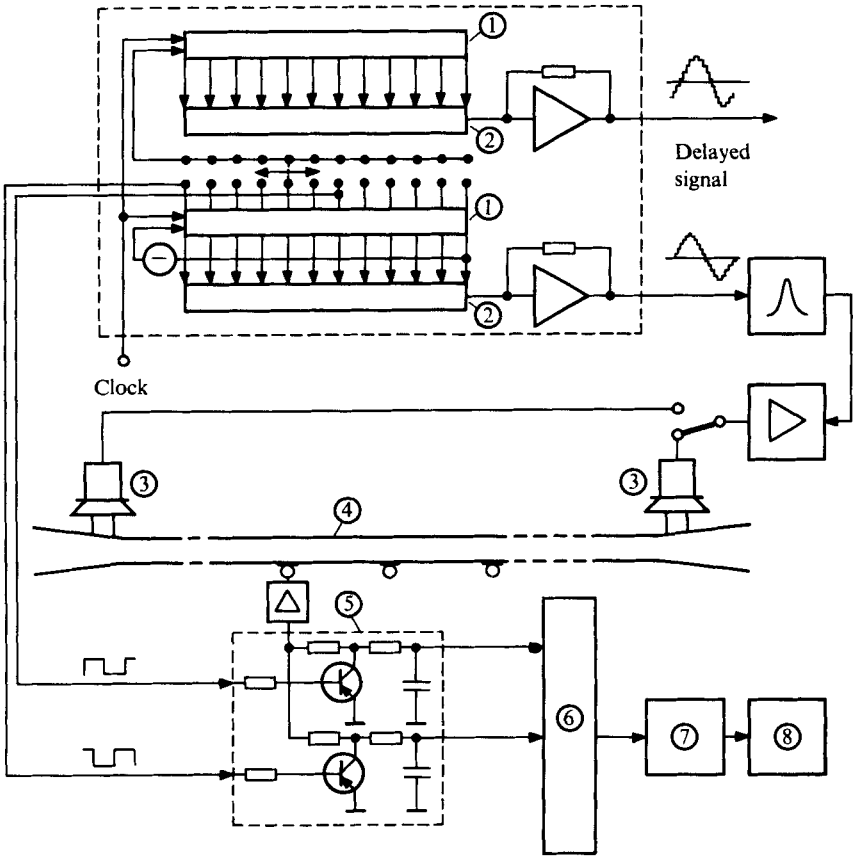

FIGURE 2. Electronic equipment for measuring and recording the amplitude and the phase of the microphone voltages. ①, 12 bit shift register; ②, resistor network for convolution of the square-wave voltage with a cosine function; ③, loudspeaker; ④, measuring pipe; ⑤, phase-sensitive rectifiers for one microphone; ⑥, multiplexer; ⑦, analog-to-digital converter; ⑧, digital magnetic tape recorder.

between the two wavenumbers: because the difference between the wavenumbers is zero in the medium at rest, one can determine the sensitivities of the microphones. Then, from the products $\tilde{p}_{\nu 1}\,\tilde{p}_{\nu 2}$, the difference between the wavenumbers can be computed.

Electronic equipment for the measurement and registration of the complex amplitudes of the microphone voltages. The amplitudes and phases of the ten rather noisy microphone voltages have to be determined simultaneously with a maximum relative error of about 10^{-3}, according to the required accuracy of the measurements. Furthermore, the data have to be recorded in a way which allows direct accessibility to the computer since extended numerical computation is needed along with the regression analysis.

The equipment sketched in figure 2 fulfils these requirements at relatively low expense. The simplest way to measure the amplitude and phase of a noisy sinusoidal voltage with complex amplitude $\tilde{U} = |\tilde{U}|\, e^{i\phi}$ is phase-sensitive rectification relative to two different phases ϕ_1 and ϕ_2. Then one obtains two d.c. voltages

$$\overline{U}_i = a_i \cos(\phi - \phi_i) + b_i, \quad i = 1, 2 \tag{5}$$

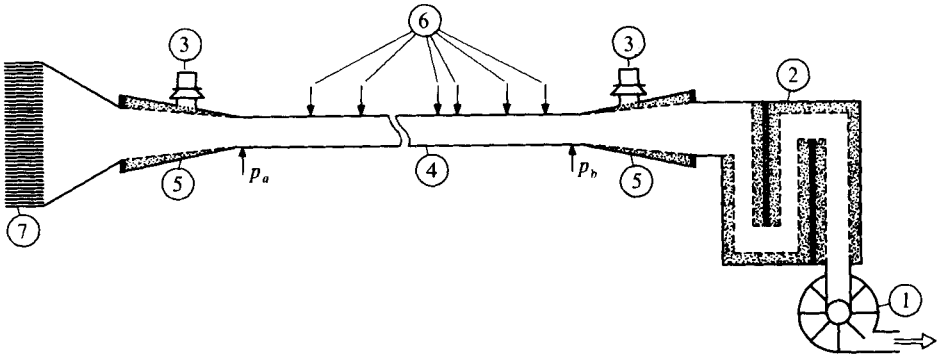

FIGURE 3. Sketch of the flow system for the sound propagation experiment. ①, fan; ②, muffler; ③, loudspeaker; ④, measuring pipe; ⑤, unechoic terminatrons; ⑥, positions for measuring static pressures and sound pressures; ⑦, flow straightener.

(b_1 and b_2 are possible offset voltages which have to be taken into account). The accuracy of $|\bar{U}|$ and of ϕ as calculated from $\bar{U}_1$ and $\bar{U}_2$ is independent of ϕ if

$$|\phi_1 - \phi_2| = \tfrac{1}{2}\pi;$$

the accuracy itself depends on the errors in the determination of a_i, b_i and ϕ_i as well as on the constancy of these parameters as a function of time. Therefore the control voltages of the rectifiers are generated by digital equipment with a highly stabilized clock. The output of the lower shift register on figure 2 is inverted and fed back to the input. Starting with all bits set to zero, a square-wave voltage consisting of twelve zero and twelve unit sections circulates. The loudspeaker voltage is obtained by filtering the fundamental frequency component out of this square wave.

The twenty phase-sensitive rectifiers are built up quite simply according to the circuit on the lower part of the figure. The RC low-pass filters have a time constant of 1 s. Small deviations from the ideal behaviour of the rectifiers ($a_1 = a_2$, $|\phi_1 - \phi_2| = \frac{1}{2}\pi$, $b_1 = b_2 = 0$) are determined by calibration voltages which are delayed by multiples of the clock period and fed to the inputs of the rectifiers. The delay is achieved by the upper shift register depicted on figure 2. The above-mentioned deviations are of the order of 10^{-2}. They depend only weakly on the frequency and they are constant for many hours. The remaining errors are smaller than 10^{-3}.

The twenty output voltages of the rectifiers are multiplexed and recorded on a digital tape recorder within a period of about 0·5 s. The tape can be directly read by the computer.

2.3. *The flow system*

The sound propagation was investigated within three pipes 70–100 diameters long (brass pipes with the inner wall polished and inner diameters of 13 mm, 20 mm and 35 mm). Figure 3 shows the flow system. The air is sucked from the laboratory. The fan noise is kept away from the measuring pipe by a muffler. Furthermore, the ends of the pipe, i.e. the conical inlet and outlet, have low acoustical reflexion coefficients. At the entrance of the flow straightener the static pressure, the temperature and the relative humidity of the air are measured. The flow parameters within the measuring pipe, i.e. the Reynolds number, the Mach number and the speed of sound, are

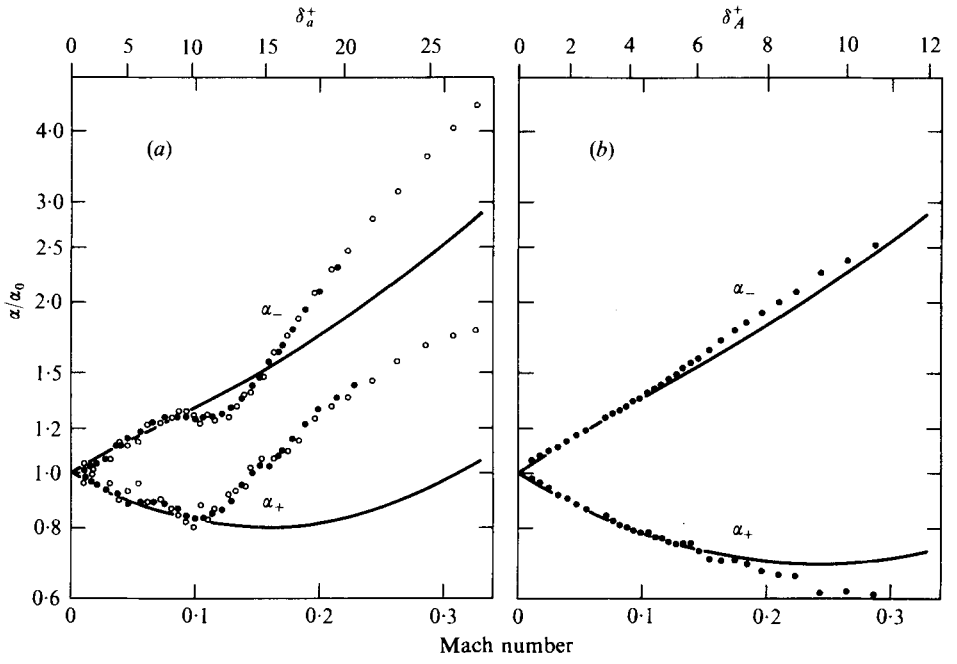

FIGURE 4. Sound attenuation in turbulent pipe flow. α_+ and α_- denote sound propagation in downstream and upstream direction, respectively. The pipe inner diameter is 20 mm. (*a*) 630 Hz, $\alpha_0 = 0{\cdot}67$ dB/m. (*b*) 3350 Hz, $\alpha_0 = 1{\cdot}56$ dB/m. The solid curves are calculated from the quasi-laminar model.

determined from these data and from the static pressures at the inlet and outlet of the pipe. For that purpose, these latter pressures p_a and p_b are 'calibrated' by measuring the static pressures at those microphone positions which lie at least 40 diameters behind the entrance of the pipe. Assuming the validity of Prandtl's drag law for circular pipes

$$c_f^{-\frac{1}{2}} = 2{\cdot}0 \log (Rc_f^{\frac{1}{2}}) - 0{\cdot}8 \tag{6}$$

(c_f = friction coefficient, $R = 2r_i \bar{u}^s/\nu_w$ = Reynolds number and $\bar{u}^s$ = flow velocity averaged over the cross-section of the pipe), one can then evaluate the Reynolds number and the Mach number of the pipe flow and calculate the two positions x_a and x_b at which one would find the pressures p_a and p_b if the turbulent pipe flow were already fully developed at the entrance of the pipe. It turns out that x_a and x_b are weakly dependent on the Reynolds number and that the pressure gradient in the leading section of the pipe (30–40 diameters long) is somewhat smaller (5 % at the most) than that in the fully developed pipe flow. The acoustical measuring section and this section of developing flow overlap (for about 20 diameters), but it is presumed that no significant error in the determination of the wall shear stress impedance is caused thereby since the deviation from fully developed flow is very small in this section of overlap.

The Mach number did not exceed 0·3 in the two narrow pipes and did not exceed 0·43 in the 35 mm pipe.

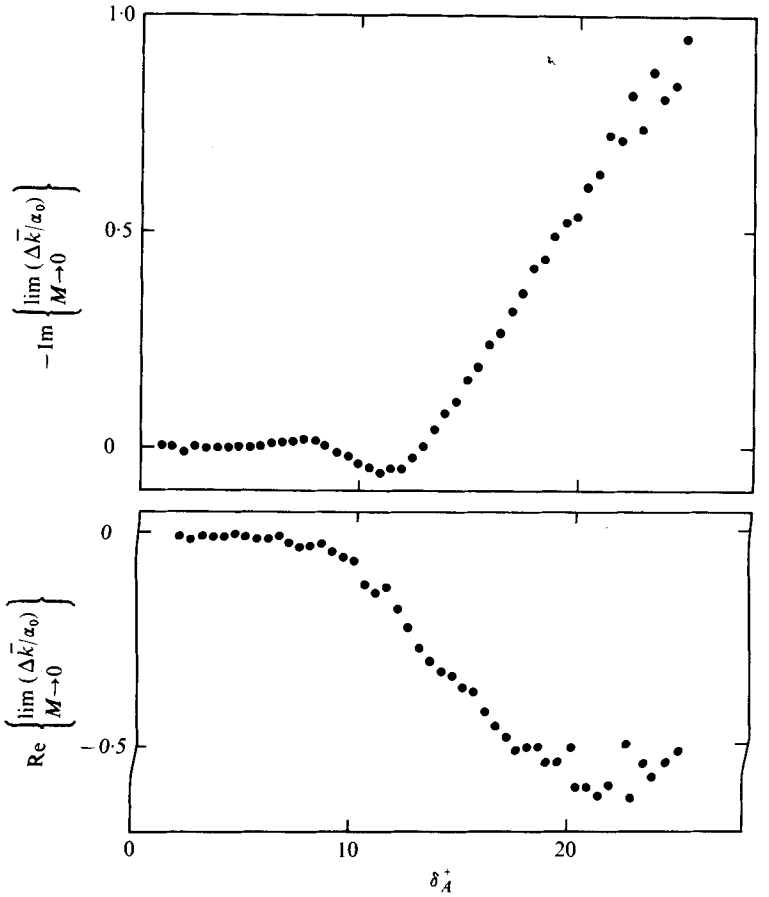

FIGURE 5. Difference between experimental and calculated values of the sound wavenumber extrapolated to zero Mach number.

2.4. *Evaluation of the data*

At low δ_A^+ ($\delta_A^+ \leqslant 15$) the variation of the normalized wall shear stress impedance Z_τ is rather small and, at high frequencies, the variation of the Mach number affects the complex sound wavenumber more significantly than the variation of Z_τ. Therefore the influence of the Mach number on the sound wavenumber was estimated by calculating the wavenumber from the turbulent flow profile while disregarding the turbulent transport of heat and of momentum. This is analogous to the quasi-laminar model used by Hussain & Reynolds (1970*a*) to demonstrate that the turbulent stresses influence the propagation of coherent perturbations of the turbulent flow. The difference between the measured and the calculated wavenumber can be associated with the variation of Z_τ and of Z_q caused by the interaction between the diffusion waves and the turbulence. Figure 4 shows, as an example, the sound attenuation in the 20 mm pipe at two frequencies as a function of the Mach number M. The attenuation in the downstream and upstream directions is denoted by α_+ and α_- respectively. The curves correspond to the calculation mentioned above. Along the top of the diagram the values of δ_A^+ are given. It is clear from the diagram that the

experimental data depart from the calculated values only at $\delta_A^+ \geqslant 5$. This agrees with the considerations concerning the propagation of the diffusion waves within the viscous sublayer (§ 1). Of course, the difference between the measured and calculated sound wavenumbers still depends on the Mach number but the difference in the wavenumbers can be extrapolated to zero Mach number far more accurately than the measured wavenumber itself. According to (2) one obtains

$$\frac{Z_\tau(\delta_A^+, R) + (\gamma - 1) Pr^{-\frac{1}{2}} Z_q(\delta_A^+, R)}{1 + (\gamma - 1) Pr^{-\frac{1}{2}}} = i \lim_{M \to 0} [\bar{k}_{\text{exp}}(M, \delta_A^+, R) - \bar{k}_{\text{cal}}(M, \delta_A^+, R)] \times r_i/\alpha_0 + 1 + i, \quad (2a)$$

$$\alpha_0 = (\omega\nu/2c^2)^{\frac{1}{2}}.$$

A dependence of the wall impedances Z_τ and Z_q on the Reynolds number was not excluded from the beginning but, at the Reynolds numbers investigated here, no significant dependence was found. In § 4.3 this subject is discussed in detail.

The wavenumber difference $\Delta\bar{k} = \bar{k}_{\text{exp}} - \bar{k}_{\text{cal}}$, averaged over both directions of sound propagation, depends on the square of the Mach number at constant δ_A^+ and R. Since M^2 is very small in the case of our measurements the terms proportional to M^4 and to higher powers of M^2 may be omitted in the Taylor series of $\Delta\bar{k}(M^2)$. Thus the extrapolation of $\Delta\bar{k}$ to $M = 0$ is simply a linear regression with respect to M^2. The result of this extrapolation is plotted on figure 5 as a function of δ_A^+. The data points represent averages with respect to the Reynolds number.

Now, according to § 2.1, the wall shear stress impedance Z_τ can be computed. The result, which is plotted on figure 12 (solid points), will be discussed in § 4. First, another experimental determination of Z_τ is described in the following section.

3. Determination of the wall shear stress impedance in a longitudinally oscillating tube containing a turbulent water flow

The determination of the wall shear stress impedance Z_τ from sound propagation in turbulent air flow through pipes is based on the assumption that the turbulent heat transport in the heat conduction wave can be calculated from data which were obtained in steady flow. Therefore it is desirable to measure Z_τ by a second experiment, more directly. (The following is partly a summary of Ahrens' thesis 1973.)

3.1. *Principle*

The idea of this experiment is to build the pipe containing the flow as a longitudinally vibrating resonator and to determine the change in Z_τ from the broadening and shift of the resonance curve. The half-width f_H of the resonance curve and the resonance frequency f_0 can be combined to give a complex resonance frequency $\Omega/2\pi = f_0 + \frac{1}{2}if_H$, which turns out to be a function of Z_τ (see § 3.2). However, the variation of Ω with Z_τ, i.e. $\partial\Omega/\partial Z_\tau$, is extremely small; therefore a very accurate experimental set-up and a sophisticated evaluation of the data are necessary.

3.2. *The resonator and the theoretical and experimental determination of* $\partial\Omega/\partial Z_\tau$

Figure 6 shows the design of the resonator. The central part is the pipe carrying turbulent water flow. The ends of this pipe are attached to the flow system. This is

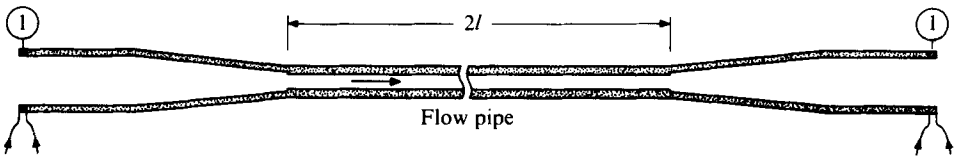

FIGURE 6. Sketch of the quartz-glass resonator. ①, PZT rings for excitation and detection of the oscillation.

possible without impairment of the resonance quality factor only if the particle velocity is zero at the points of attachment. For this purpose, the length of the outermost cylindrical pieces of the resonator, and thereby the resonance frequency, is so adjusted that the length of the pipe carrying the flow equals half a wavelength of the longitudinal wave. So the particle velocity in the axial direction is a maximum in the mid-portion of the pipe. The dimensions of the pipe (inner diameter = 6·5 mm, length = 400 mm and f_0 = 7·35 kHz) were chosen to attain the highest possible values of δ_A^+ for the maximum driving pressure (40 atm) and the maximum flow rate (1800 cm³/s).

The resonator is made of quartz glass, which is advantageous for several reasons. First of all, this material has a high acoustical quality factor and the resonator can easily be fabricated with smooth and resistant surfaces. Furthermore, the lateral contraction is small and the sound speed is high; so the coupling between the oscillation of the resonator and the water-born sound is small: variations of the complex resonance frequency Ω caused by the sound radiation into the flow system are nearly incalculable. Last but not least, the material is transparent; thus, for example, the onset of cavitation can be observed; cavitation within the measuring pipe must be avoided since the strong interaction between the water-born sound and the cavitation bubbles results in substantial changes in Ω.

The oscillation of the resonator and of the water column was calculated to obtain a general view of the dependence of the complex resonance frequency on the wall shear stress impedance Z_τ and on the sound radiation into the flow system. The calculation is summarized in the appendix; it yields

$$\delta\Omega = \frac{ic_t'}{l_{\mathrm{tot}}}\left\{ Z_\tau \frac{\rho_w\left(\frac{\omega\nu}{2}\right)}{\rho_t c_t'}\frac{2lr_i}{r_o^2-r_i^2}\frac{\left(\frac{c_t}{c_w}\right)^2-1+\frac{4}{m}+2\frac{\rho_w}{\rho_t}\left(\frac{r_o^2+r_i^2}{r_o^2-r_i^2}+\frac{1}{m}\right)}{\left(\frac{c_t}{c_w}\right)^2-1+2\frac{\rho_w}{\rho_t}\left(\frac{r_o^2+r_i^2}{r_o^2-r_1^2}+\frac{1}{m}-\frac{2}{m^2}\frac{r_1^2}{r_o^2-r_1^2}\right)} + \frac{\frac{8}{m^2}\frac{\rho_w}{\rho_t}\frac{r_i^2}{r_o^2-r_i^2}\frac{c_t'}{c_w'}}{\left[\left(\frac{c_t}{c_w}\right)^2-1+2\frac{\rho_w}{\rho_t}\left(\frac{r_o^2+r_i^2}{r_o^2-r_i^2}+\frac{1}{m}\right)\right]^2} \times \frac{1+iw\tan k_w l-2\delta_L^2}{(w+i\tan k_w l)(1+iw\tan k_w l)-2i\delta_L^2\tan k_w l}\right\} \tag{7}$$

(w and δ_L characterize the water sound impedances at the ends of the measuring pipe; for their definitions and for the rest of the notation see the appendix). Equation (7) indicates that the part of $\delta\Omega$ caused by water sound radiation into the flow system ($\delta\Omega_w$) may by far exceed the part due to the excitation of the shear wave ($\delta\Omega_\tau$). This

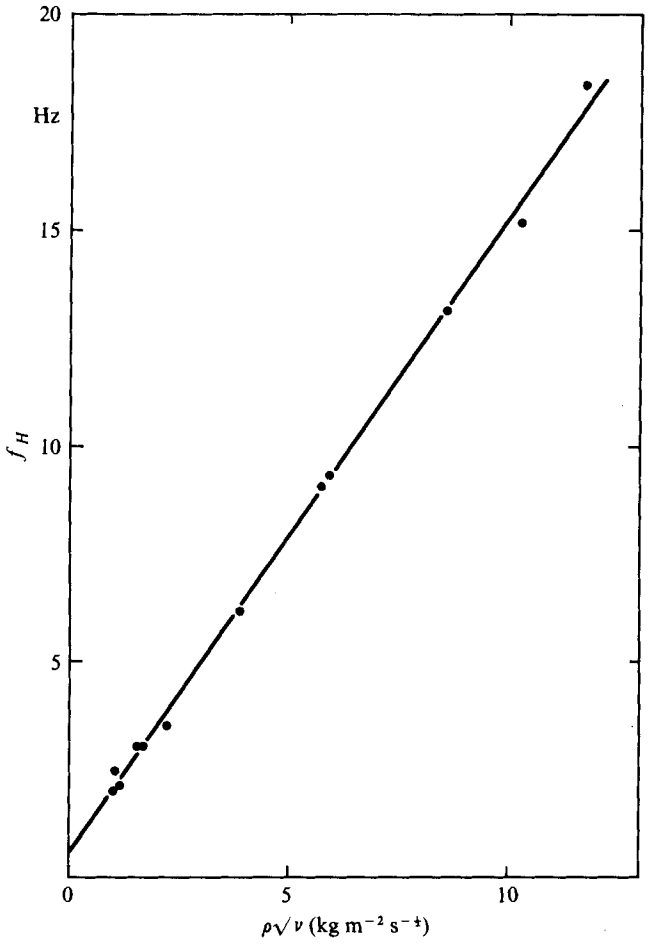

FIGURE 7. Half-width of the resonance curve of the resonator when filled with various mixtures of glycerin and water. The slope of the straight line has the theoretical value.

may be seen more clearly from the ratio of these two parts of $\delta\Omega$ in the case of equal radiation impedances at both ends of the measuring pipe (i.e. $\delta_L = 0$):

$$|\delta\Omega_w/\delta\Omega_t| = 0{\cdot}76/|w + i\tan k_w l|. \tag{8}$$

The numerical factor is valid for the actual resonator and for water at rest. In spite of the low Poisson number of quartz glass there exists an extended range of radiation impedances w in which $|\delta\Omega_w/\delta\Omega_r|$ is considerable. At $w = -i\tan(k_w l)$ the water column within the measuring pipe has a resonance; then (7) is not valid. A more rigorous calculation reveals that in this case $\delta\Omega$ can no longer be split into two parts depending on Z_r and on w, respectively, and that, in any case, the quality factor of the resonator decreases drastically. The latter fact was used to avoid this critical radiation impedance; the impedance at the outlet of the measuring pipe was varied to yield the maximum possible quality factor of the resonator. It is very likely that $|\delta\Omega_w|$ as well as $|\partial(\delta\Omega_w)/\partial w|$ is small in this case. So small changes in w due to the variation of the flow velocity do not cause any noticeable changes in Ω. Equation (7) contains a

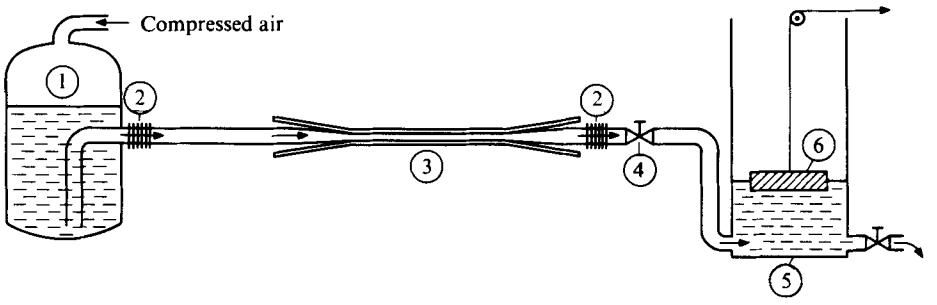

FIGURE 8. Flow system for the resonator experiment. ①, pressure tank; ②, flexible pipe; ③, resonator; ④, valve; ⑤, collecting tank; ⑥, swimmer driving a precision potentiometer.

further quantity which cannot be determined except at high computational expense, i.e. the effective length l_{tot} of the total resonator. Therefore we decided to determine $\partial(\delta\Omega)/\partial Z_\tau$ experimentally. For this purpose the measuring pipe was filled with various glycerin–water mixtures. Then the half-width of the resonance curve should be a linear function of $\rho\nu^{\frac{1}{2}}$, according to (7) (disregarding the small influence of the sound speed, which depends slightly on the mixing ratio). The measured half-width is plotted on figure 7 as a function of $\rho\nu^{\frac{1}{2}}$. The slope of the plotted straight line is computed from (7) assuming that the effective length of the resonator equals its actual length. Obviously this assumption is justified.

3.3. *Flow system*

Figure 8 shows a sketch of the flow system. Water contained in a pressure tank is driven through the resonator pipe by compressed air. A cylindrical tank collects the water. So the flow velocity in the measuring pipe may be determined from the rise of the water level in that tank. A maximum driving pressure of about 40 atm is necessary to yield the required flow velocity of about 50 m/s, and thereby two problems arise.

(*a*) The junction between the resonator and the flow system has to be leakproof at such high pressures and, on the other hand, the quality factor of the resonator must be essentially unimpaired by this junction.

(*b*) The static pressure is rather small at the outlet of the measuring pipe. This leads to cavitation, which influences the complex resonance frequency of the resonator rather strongly, as mentioned above.

Figure 9 shows how these problems were overcome. Two rings of UHU-PLUS, a two-component cement, were glued to the ends of the measuring pipe. After curing, the sharpened ends of the tapered water supply pipes were pressed into the slightly yielding cement. It turned out that the quality factor of the resonator was practically unaffected by this procedure and, which is more important, that the complex resonance frequency was only weakly dependent on the water pressure.

The increase in the pressure in the outlet diffuser leads to a low pressure at the end of the measuring pipe. Therefore a flow resistance had to be installed at the outlet of the diffuser. Furthermore, various pipe fittings were inserted into the diffuser. So the water sound impedance at the outlet of the measuring pipe was varied to yield a value which was far from the critical impedance (see § 3.2).

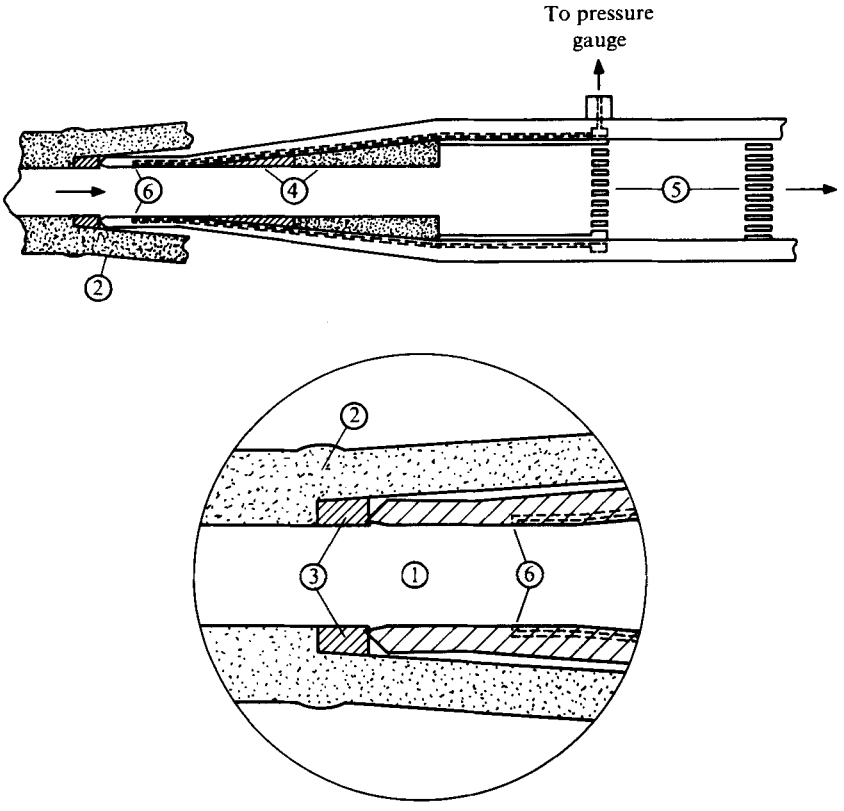

FIGURE 9. Sketch of the junction ① between the resonator ② and the flow system (③ is ring of UHU-PLUS). The pipe fittings ④ and the flow resistances ⑤ in the outlet diffuser are present to suppress cavitation and to adjust the optimum water sound impedance at the outlet of the pipe. – – –, borings ⑥ and channels for measuring the static pressure.

The static pressures at the inlet and at the outlet of the resonator pipe were measured through narrow borings in the tapered water supply pipes as depicted on figure 9. Two piezoelectric transducers served as pressure gauges. The static pressure gradient in the measuring pipe, as determined from these pressures, was somewhat higher (about 6 %) than that predicted by Prandtl's formula (6). From the pressure gradient dp/dx, the friction velocity u_τ was computed according to

$$u_\tau = \left(\frac{dp}{dx}\frac{r_i}{2\rho}\right)^{\frac{1}{2}}. \tag{9}$$

3.4. *Electronic equipment*

The measuring time is limited by the ratio of the pressure-tank volume to the flow rate. Therefore it was necessary to measure and to record the data automatically. Figure 10 shows the electronic equipment. The oscillation of the resonator was excited and picked up by two piezoelectric rings (PZT-rings) attached to both ends of the

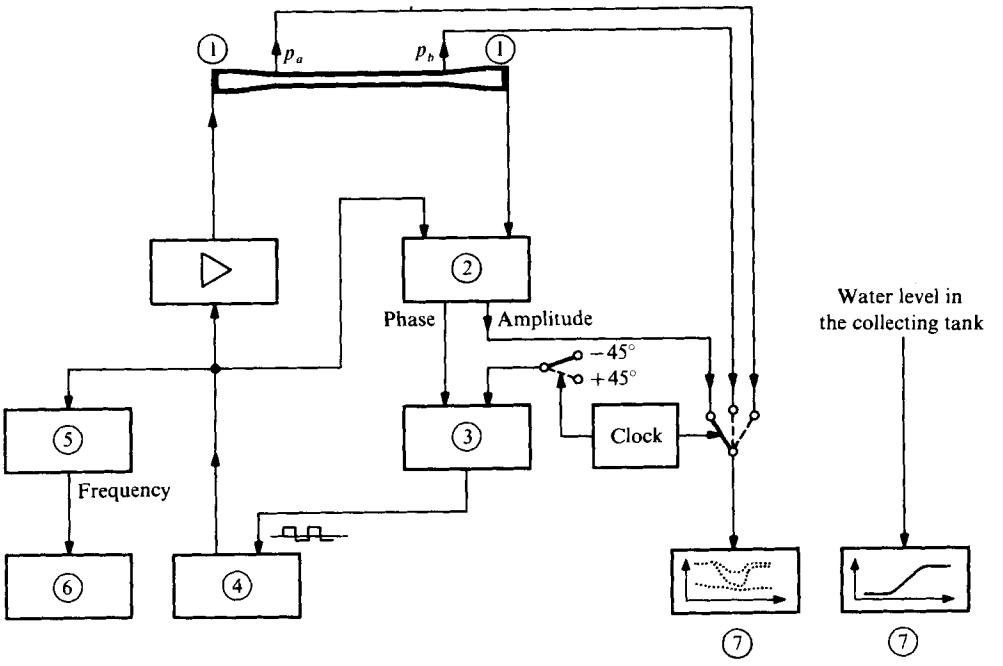

FIGURE 10. Electronic equipment for the automatic measurement of the complex resonance frequency. ①, PZT rings; ②, two-phase lock-on amplifier; ③, integral controller; ④, voltage-controlled oscillator; ⑤, frequency counter; ⑥, printer; ⑦, Y, T recorder.

resonator. The (complex) ratio of the output voltage $\tilde{U}_o$ to the input voltage $\tilde{U}_i$ is given by

$$\tilde{U}_o/\tilde{U}_i = \frac{C}{\omega - \Omega}. \tag{10}$$

C is a slightly varying complex function of ω and may be regarded as constant in the narrow range of frequencies considered here. The '45° frequencies' $\omega_1 = 2\pi(f_o - \frac{1}{2}f_H)$ and $\omega_2 = 2\pi(f_o + \frac{1}{2}f_H)$ are characterized by the fact that the phase difference between $\tilde{U}_o$ and $\tilde{U}_i$, i.e. $\phi(\tilde{U}_o/\tilde{U}_i)$, is shifted by 90° if one proceeds from $\omega = \omega_1$ to $\omega = \omega_2$:

$$\phi\left[\frac{\tilde{U}_o}{\tilde{U}_i}(\omega_1)\right] - \phi\left[\frac{\tilde{U}_o}{\tilde{U}_i}(\omega_2)\right] = \frac{\pi}{2}. \tag{11}$$

Furthermore, the absolute values $|\tilde{U}_o/\tilde{U}_i|$ are equal at the 45° frequencies. The phase differences $\phi[(\tilde{U}_o/\tilde{U}_i)(\omega_1)]$ and $\phi[(\tilde{U}_o/\tilde{U}_i)(\omega_2)]$ are practically independent of Ω. This fact is used to adjust the 45° frequencies automatically with the aid of a phase meter, an integral controller and a voltage-controlled oscillator, as sketched on figure 10. An automatic switch ensures that ω_1 and ω_2 are adjusted alternately. The adjusted frequencies are measured by a frequency counter and recorded by a printer. For monitoring purposes the amplitude $|\tilde{U}_o|$ is measured then $|\tilde{U}_o|$ and the static pressures at the ends of the measuring pipe are multiplexed and recorded on a Y, T recorder. A second Y, T recorder records the water level in the collecting tank.

3.5. *Measuring procedure and evaluation of the data*

The variation of the wall shear stress impedance Z_τ is rather small in the range of δ_A^+ covered by our experimental set-up. So the change $\delta\delta\Omega(\delta_A^+)$ in the complex resonance frequency caused by the variation of Z_τ is extremely small (of the order of 0·1 Hz). Therefore the measurements have to be conducted very carefully. First, the valve at the outlet of the resonator is shut (figure 8) and the pressure tank as well as the measuring pipe are pressurized up to the desired driving pressure. By briefly opening the valve, air bubbles possibly left in the flow system are washed away. Then the resonance frequency Ω_1 and the static pressure p_1 are measured. When, after opening the valve, the flow has become steady, the new resonance frequency Ω_2, the static pressures p_{2a} and p_{2b} at the inlet and the outlet of the measuring pipe as well as the other quantities are recorded. Finally, after shutting the valve again, the resonance frequency Ω_3 and the pressure p_3 are determined.

Several assumptions are necessary to evaluate $\delta\delta\Omega(\delta_A^+)$ from these data, i.e. to eliminate the influence of the static pressure on the complex resonance frequency. It is reasonable to assume that the observed influence of the static pressure on the resonance frequency results from some action of the pressure on the junctions between the resonator and the flow system. Furthermore, it is assumed that the variations of the resonance frequency caused by variations of the pressure ($\delta\Omega_{pa}$, $\delta\Omega_{pb}$) and by variations of Z_τ ($\delta\delta\Omega$) are additive, i.e.

$$\Omega(\delta_A^+, p_a, p_b, t) = \Omega_o(t) + \delta\Omega_{pa}(p_a) + \delta\Omega_{pb}(p_b) + \delta\delta\Omega(\delta_A^+). \tag{12}$$

$\Omega_o(t)$ is a slowly varying function of time containing all unpredictable changes in the resonance frequency. A more constricting assumption is

$$\delta\Omega_{pa} \equiv \delta\Omega_{pb} \equiv \delta\Omega_p. \tag{13}$$

Then one obtains

$$\begin{aligned}
\Omega_1 &= \Omega_o(t_1) + 2\delta\Omega_p(p_1),\\
\Omega_2 &= \Omega_o(t_2) + \delta\Omega_p(p_{2a}) + \delta\Omega_p(p_{2b}) + \delta\delta\Omega(\delta_A^+),\\
\Omega_3 &= \Omega(t_3) + 2\delta\Omega_p(p_3).
\end{aligned}$$

Finally, it is reasonable to take $\Omega_o(t_2) = \frac{1}{2}[\Omega_o(t_1) + \Omega_o(t_3)]$, which yields

$$\delta\delta\Omega(\delta_A^+) = \Omega_2 - \tfrac{1}{2}(\Omega_1 + \Omega_3) - \delta\Omega_p(p_{2a}) - \delta\Omega_p(p_{2b}) + \delta\Omega_p(p_1) + \delta\Omega_p(p_3). \tag{14}$$

The data were evaluated according to this equation. $\delta\Omega_p$ was determined from the data taken at zero flow velocity. Assuming that $\Omega_o(t)$ fluctuates irregularly, one obtains

$$\delta\Omega_p(p) = \overline{\Omega(0,p,p,t)}^t - \overline{\Omega(0,0,0,t)}^t.$$

The mean values are meaningful since the data for a definite pressure were measured at many different times.

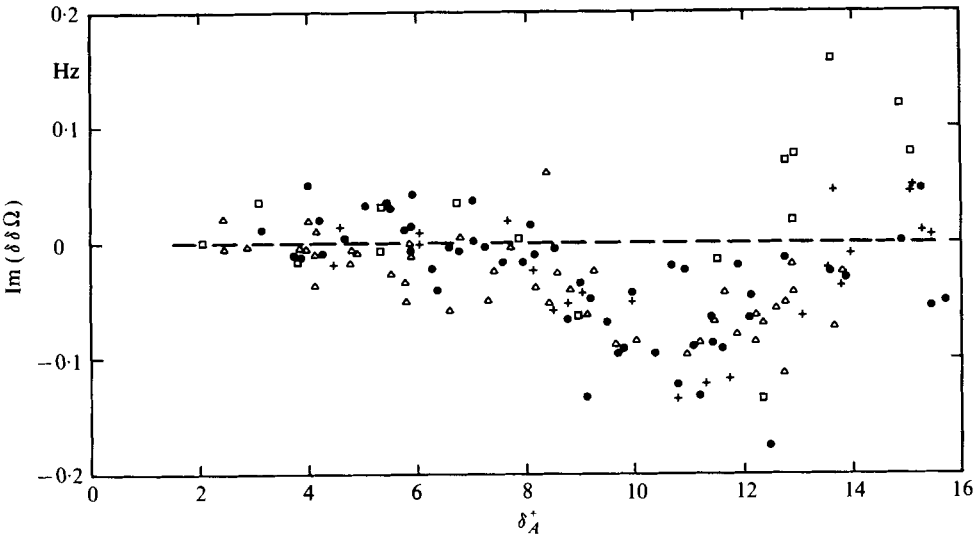

FIGURE 11. Variation of the imaginary part of the resonance frequency caused by the interaction between the shear wave and the turbulence. The various symbols denote various experimental conditions.

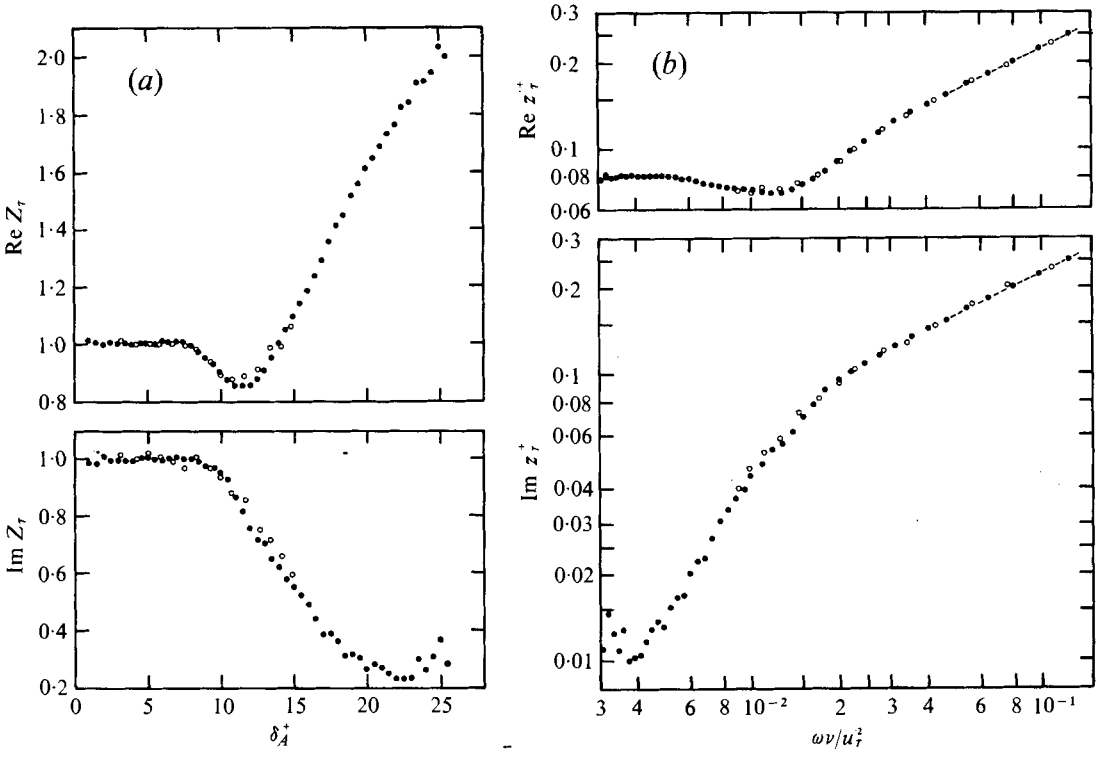

FIGURE 12. (*a*) Normalized wall impedance $Z_\tau = z_\tau(\frac{1}{2}\omega\rho\mu)^{-\frac{1}{2}}$ of the shear wave as a function of $\delta_A^+ = (2u_\tau^2/\nu\omega)^{\frac{1}{2}}$. ●, sound propagation; ○, oscillating pipe. (*b*) Same data as in (*a*); here the wall shear stress impedance is normalized to ρu_τ and plotted as a function of the 'inner Strouhal number' $\omega\nu/u_\tau^2$. The dashed straight lines correspond to $Z_\tau = 1 + i$.

Figure 11 shows Im ($\delta\delta\Omega$) as a function of δ_A^+, which is computed from the pressure drop in the measuring pipe according to (1) and (9):

$$\delta_A^+ = \left(\frac{p_{2a} - p_{2b}}{\rho\omega\nu}\frac{r_t}{2l}\right)^{\frac{1}{2}}. \tag{15}$$

The different symbols indicate the different series of measurements conducted after renewed clamping of the resonator between the inlet pipe and the outlet diffuser. $\delta\Omega_p(p)$ turned out to be quite different in each of these four cases. Yet the resulting values of $\delta\delta\Omega$ show no significant differences. So, obviously, the assumptions leading to (14) are adequate. Furthermore, the flow resistance in the outlet diffuser was varied without any effect on $\delta\delta\Omega$. Figure 12 shows $Z_\tau(\delta_A^+)$ (open circles), which was determined, according to (7), from averaged values of $\delta\delta\Omega(\delta_A^+)$.

4. Discussion of the measurements

4.1. *Results*

The normalized wall shear stress impedance Z_τ obtained from the two experiments described above is plotted on figure 12(*a*) as a function of the frequency parameter δ_A^+. While the variables Z_τ and δ_A^+ were chosen because of their close relation to our experimental conditions (fixed frequency, variation of the flow velocity), a more common frequency parameter is the Strouhal number $\omega\nu/u_\tau^2 = 2/(\delta_A^+)^2$. Therefore the wall shear stress impedance is also plotted as a function of the Strouhal number, on figure 12(*b*); the impedance is normalized here by ρu_τ, which is independent of the frequency ($z_\tau^+ = Z_\tau/\delta_A^+$). As mentioned above, a possible dependence on the Reynolds number was disregarded in these diagrams, and the values depicted here are averaged with respect to the Reynolds number. The good agreement between the results of the two quite different measuring methods is encouraging and supports the adequacy of the assumptions on which the evaluation of the measurements is based. These assumptions are essentially that in the case of the resonator experiment (§ 3) the water sound radiation into the flow system may be disregarded under the special conditions of the measurements and, more fundamental, that in the case of the sound propagation experiment (§ 2) the turbulent heat transport is controlled by the local temperature gradient independently of the frequency in the range of Strouhal numbers considered here.

The measurement accuracy at $\delta_A^+ < 15$ may be estimated from the scatter of the measured results, especially from the differences between the two measuring methods. At $\delta_A^+ > 15$, data were obtained only from the sound propagation experiment. In particular, the error in Im Z_τ is likely to be rather large since Im Z_τ is determined from small changes in the phase velocity of the sound wave. So small errors in the Mach number ($\Delta M/M \approx 5 \times 10^{-3}$) lead to rather large errors in Im Z_τ (about 2×10^{-1} at $\delta_A^+ = 25$). Thus it is open to question whether Im Z_τ increases at high δ_A^+, again, as it seems to. Moreover, the error due to the uncertainty in the Mach number decreases with decreasing δ_A^+ approximately in proportion to $(\delta_A^+)^2$.

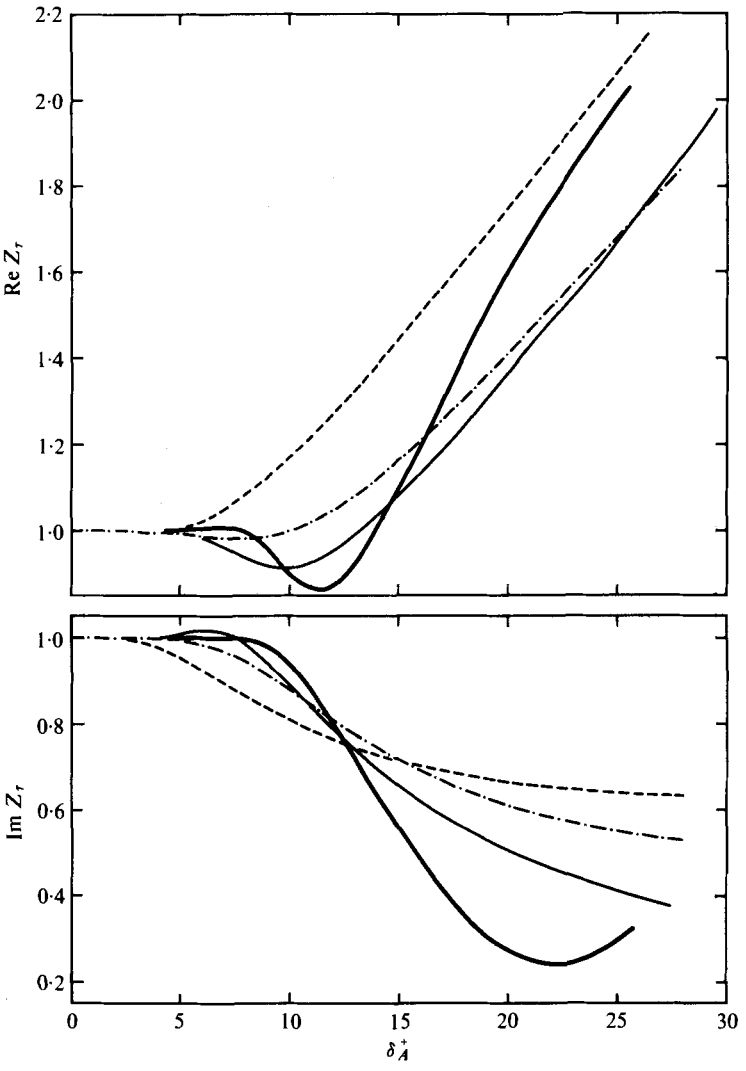

FIGURE 13. Normalized wall impedance of the shear wave computed on the basis of various models of the interaction between the shear wave and the turbulence. ——, rigid-plate model ($d^+ = 15$); – – –, eddy-viscosity model; –·–·–, eddy-viscoelasticity model; ——, experimental data.

4.2. *Interpretation of the results*

A qualitative explanation of the trend of $Z_\tau(\delta_A^+)$ can easily be given. At low δ_A^+ (high Strouhal numbers) the shear wave decays essentially within the viscous sublayer. So, as mentioned in § 1, no influence of the turbulent transport of momentum on the wall impedance of the shear wave is possible and $Z_\tau = 1 + i$ as for the medium at rest (see figure 12*a*). At high values of δ_A^+, however, the viscous sublayer and the transition region are thin compared with the shear wavelength. Then, in a rough approximation one may simulate the turbulence by a rigid plate at some distance d from the wall (regarding the shear wave as being excited by oscillations of the wall); d corresponds to the thickness of the viscous sublayer. So, at low Strouhal numbers, z_τ as well as

z_τ^+ should be independent of the frequency, which implies that the imaginary part of the shear stress impedance tends to zero (see figure 12*b*).

It is interesting to note that this very rough model of the interaction between the shear wave and the turbulence yields a trend for $Z_\tau(\delta_A^+)$ which is in qualitative agreement with the experimental results over the entire range of δ_A^+ (see figure 13). The minimum of Re Z_τ at $\delta_A^+ \approx 11$ is caused by interference between the shear wave excited at the oscillating wall and the wave which is reflected from the rigid plate. The depth of the minimum depends on the magnitude of the reflexion coefficient as well as on its phase, because of the high attenuation of the shear wave. At the hypothetical rigid plate, the shear wave is totally reflected. However, the reflexion at the turbulence must be considered to take place not at a definite plane but in a more or less extended layer. So, in reality, the reflexion coefficient is smaller than unity owing to interference effects depending mainly on the thickness of the reflecting layer compared with the shear wavelength. The minimum of Re Z_τ tends to be less pronounced because of the effect of this smeared reflexion, but the quasi-elastic properties of the turbulence, as predicted by Davis (1974) and many others, will shift the phase of the reflexion coefficient such that the minimum of Re Z_τ becomes deeper. These trends may be viewed on figure 13; there the wall shear stress impedance is plotted as a function of δ_A^+, as computed from three different models. The thin solid curves depict the rigid-plate model mentioned above; $d^+ = 15$ was chosen to fit the experimental data, which are represented by the thick solid curves. The dashed curves result from the assumption that the turbulent transport of momentum can be described by an eddy viscosity whereas the dash–dot curves were computed on the basis of the eddy viscoelasticity, which was approximated by Davis (1974).

The eddy viscosity was determined from Prandtl's mixing-length hypothesis assuming that the mixing length l_m itself is not modulated by the shear wave. This yields an effective kinematic viscosity

$$\nu_{\text{eff}} = \nu + 2l_m^2 \,|d\bar{u}/dy|. \tag{16}$$

The mixing length in the transition region is computed from van Driest's (1956) hypothesis

$$l_m = \kappa y(1 - e^{-\frac{1}{26}y^+}) \tag{17}$$

($\kappa = 0{\cdot}4$ is Kármán's constant and y = distance from the wall). Reynolds & Hussain (1972) have used an eddy viscosity which is half that in (16); they assumed that the turbulence energy is not modulated by the coherent perturbation of the turbulent flow.

The eddy-viscoelasticity model of Davis (1974) is confined to the fully turbulent region of the boundary layer. So the application of this model to the transition region is more or less to be considered as a demonstration of the trend which is caused by the quasi-elastic behaviour of the turbulence. The eddy viscoelasticity normalized by the eddy viscosity in steady flow is proportional to the ratio $\overline{v'^2}/\overline{u'v'}$ of the normal (y-direction) stress to the shear stress; at low Reynolds numbers this was roughly modelled by

$$\overline{v'^2}/\overline{u'v'} = 1{\cdot}7 \tanh \tfrac{1}{40}y^+$$

according to data measured by Reichardt (1951) and Eckelmann (1970). At high Reynolds numbers somewhat smaller values of this stress ratio are expected.

The calculation of the wall shear stress impedance is based on the momentum equation for the complex amplitude $\tilde{u}$ of the velocity with $\partial/\partial x = \partial/\partial z = 0$:

$$i\omega\tilde{u} = \frac{d}{dy}\left(\nu_{\text{eff}}\frac{d\tilde{u}}{dy}\right) = 0. \tag{18}$$

Assuming

$$\tilde{u}(y) = \tilde{u}_0 \exp\left(-\int_0^y \gamma_\tau(y')\,dy'\right) \tag{19}$$

yields

$$\frac{d\gamma_\tau}{dy} = \gamma_\tau^2 - \gamma_\tau \frac{1}{\nu_{\text{eff}}}\frac{d\nu_{\text{eff}}}{dy} - \frac{i\omega}{\nu_{\text{eff}}}. \tag{20}$$

This differential equation is integrated numerically starting with the approximation

$$\gamma_\tau(y_s) \approx (1+i)\left(\frac{\omega}{2\nu_{\text{eff}}}\right)^{\frac{1}{2}} + \frac{1}{4\nu_{\text{eff}}}\frac{d\nu_{\text{eff}}}{dy} \tag{21}$$

at sufficiently large y_s. Finally one obtains

$$Z_\tau = \delta_A \gamma_\tau(0). \tag{22}$$

The agreement between these computed wall shear stress impedances and the experimental data is only qualitative (figure 13) and there is no trend towards better agreement if one proceeds from the crude solid-plate model of the turbulence to the somewhat more realistic eddy-viscosity model then to the eddy-viscoelasticity model.

According to (18)–(22), the wall shear stress impedance $Z_\tau(\delta_A^+)$ is a functional of the effective viscoelasticity $\nu_{\text{eff}}(y^+, \delta_A^+)$ provided that the turbulence may be described by such a simple constitutive law. However, it is not possible to determine $\nu_{\text{eff}}(y^+, \delta_A^+)$ from the measured $Z_\tau(\delta_A^+)$ without any further assumptions. Nevertheless, the deep minimum of Re Z_τ at $\delta_A^+ \approx 12$ indicates that the reflexion of the shear wave at the edge of the viscous sublayer is confined to a layer which is much thinner than that predicted by the last two models described above.

Higher-order closure models have been applied to oscillatory flow through ducts, especially models which are based on the transport equation for the turbulent kinetic energy. Vasiliev & Kvon (1971), for example, calculate the oscillatory flow in a pipe. However, they evaluate their model at large amplitudes of the mean-flow velocity oscillation, obtaining wall shear stresses which are far from the experimental values obtained here (figure 12). Acharya & Reynolds (1975) have compared the predictions from a similar model with experimental data which were obtained in a two-dimensional channel flow with superimposed small amplitude oscillations of the mean-flow velocity, and found large discrepancies. Acharya & Reynolds conclude that the pressure–strain correlation is a crucial term which affects the dynamics of the Reynolds stresses. This means that the turbulent shear stress caused by small amplitude perturbations cannot be described by an eddy viscosity or an eddy viscoelasticity (which are local quantities, whereas the pressure is a functional of the total velocity field).

4.3. *Dependence on the Reynolds number*

The question of whether the wall shear stress impedance depends on the Reynolds number is closely related to the question of whether the dynamics of the Reynolds

stresses in the inner layer are influenced by interactions between the inner layer and the outer layer. A coupling between the inner and the outer layer has become obvious through investigation of the bursting phenomenon which was observed by Kline *et al.* (1967) in the viscous sublayer. Laufer & Badri Narayanan (1971) as well as Rao, Narasimha & Badri Narayanan (1971) found that the mean rate of occurrence of the bursting phenomenon depends on outer variables rather than on the inner parameters of the turbulent boundary layer. Acharya & Reynolds (1975) found a rather peculiar dependence of the coherently oscillating velocity component $\tilde{u}$ on the distance from the wall when the frequency of a velocity oscillation superimposed upon a two-dimensional channel flow was near the mean bursting frequency, and they suggest that this coincidence might be of importance. According to Laufer & Badri Narayanan (1971), the mean bursting frequency is given by

$$\omega_B \approx \tfrac{2}{5}\pi\,\overline{u}_m/r_i, \tag{23}$$

where $\overline{u}_m$ is the centre-line velocity. This yields a corresponding quantity

$$\delta_{AB}^+ \approx 0{\cdot}3(Rc_f)^{\frac{1}{2}}, \tag{24}$$

where c_f is the drag coefficient for turbulent pipe flow according to (6) and R is the Reynolds number based on the diameter and the flow velocity $\overline{u}^s$, which is the average over the cross-section. The weak dependence of $\overline{u}^s/\overline{u}_m$ on the Reynolds number has been disregarded.

Another reason for a possible dependence on the Reynolds number of the wall shear stress impedance is the fact that, at low Reynolds numbers, the gap between the edge of the viscous sublayer and the outer portion of the boundary layer becomes narrow, and that, in any case, the shear wave may penetrate into the outer layer when δ_A^+ becomes sufficiently large. Then the flow tends to follow quasi-steadily the oscillations of the wall. In this case the wall shear stress impedance depends additionally on 'external' conditions, such as whether (*a*) the axial pressure gradient dp/dx in the pipe is kept constant or (*b*) the flow rate through the pipe is a constant. Condition (*a*) leads to

$$\lim_{\delta_A^+\to\infty} Z_\tau = 0, \quad \partial^2 p/\partial x\,\partial t = 0 \tag{25}$$

and condition (*b*) yields at very large δ_A^+

$$Z_\tau = -\frac{\partial\overline{\tau}_w}{\partial\overline{u}^s}\left(\frac{2}{\omega\rho\mu}\right)^{\frac{1}{2}} = \frac{(\frac{1}{2}c_f)^{\frac{1}{2}}\ln 10}{\ln 10+(2c_f)^{\frac{1}{2}}}\,\delta_A^+, \quad \frac{\partial\overline{u}^s}{\partial t} = 0. \tag{26}$$

Thus Z_τ depends on the Reynolds number in this case.

A quantity δ_{AC}^+ will now be estimated which is such that $Z_\tau(\delta_A^+)$ is independent of R at $\delta_A^+ \ll \delta_{AC}^+$ (apart from a possible coupling between the inner and the outer layer) and such that the flow is quasi-steady at $\delta_A^+ \gg \delta_{AC}^+$. The shear wavelength should be comparable with the pipe radius at $\delta_A^+ = \delta_{AC}^+$, and a reasonable estimate is

$$\int_0^{r_i} \mathrm{Re}\,[\gamma_\tau(y,\delta_{AC}^+)]\,dy = 1. \tag{27}$$

$\gamma_\tau(y,\delta_{AC}^+)$ is approximated by the first term of (21) and, at the low Strouhal numbers corresponding to δ_{AC}^+, ν_{eff} is assumed to be twice the eddy viscosity in steady flow, according to (16). Then the integral in (27) should be proportional to $(r_i^+/\delta_{AC}^+)\,R^{-\frac{1}{2}}$

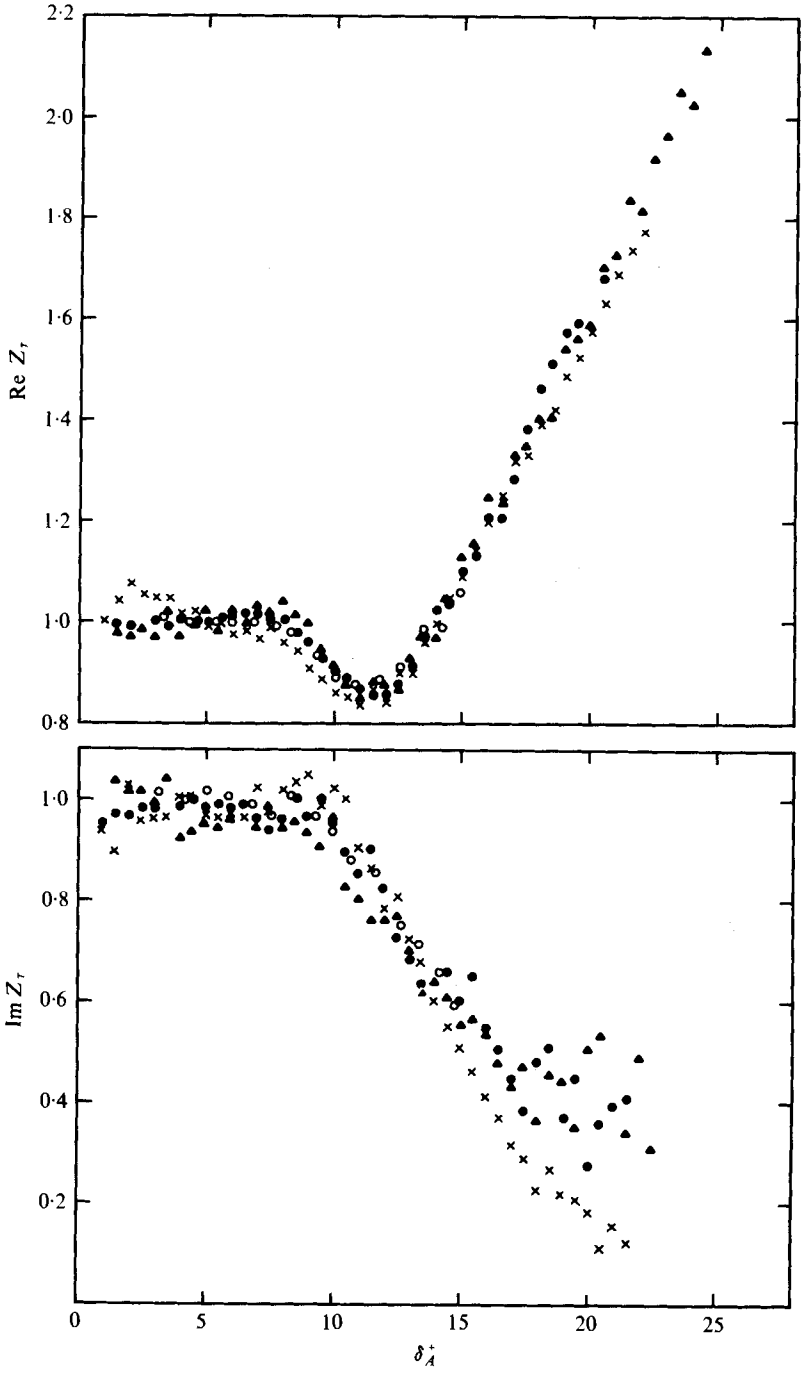

FIGURE 14. Normalized wall shear stress impedance evaluated from measurements in different pipes. Sound propagation in air: ×, $2r_i = 13$ mm; ●, $2r_i = 20$ mm; ▲, $2r_i = 35$ mm. Oscillating pipe carrying water flow: ○, $2r_i = 6{\cdot}5$ mm.

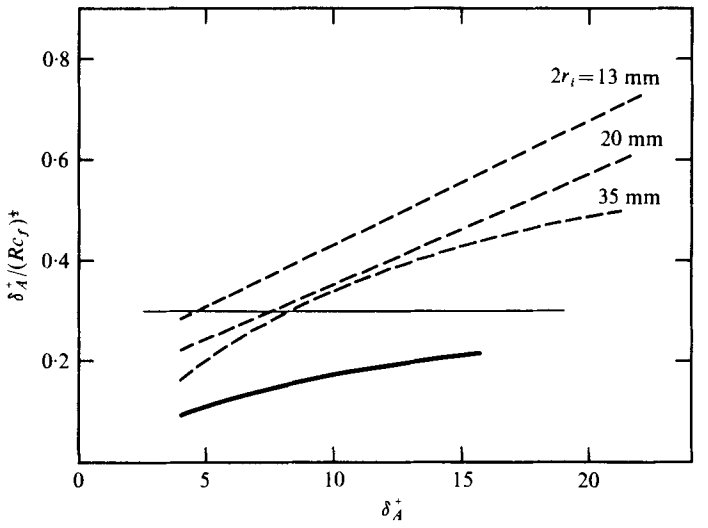

FIGURE 15. Relation between the outer and the inner variables of the boundary layer for the data of figure 14. – – –, estimates for the sound propagation experiment; ——, oscillating pipe experiment. At $\delta_A^+(Rc_f)^{-\frac{1}{2}} = 0{\cdot}3$ the frequency of the shear wave and the mean bursting frequency coincide.

(scaling the eddy viscosity by outer variables). Introducing data for the eddy viscosity measured by Reichardt (1951), (27) yields

$$\delta_{AC}^+ \approx 3(Rc_f)^{\frac{1}{2}}. \tag{28}$$

Again, $\overline{u}^s/\overline{u}_m$ has been assumed to be constant. By the way, the same result is obtained if one considers the distance from the inlet of a pipe and the corresponding time which a turbulent pipe flow needs to become fully developed.

Thus, according to (24) and (28), a possible influence of the outer variables on the wall shear stress impedance is described by the ratio $\delta_A^+/(Rc_f)^{\frac{1}{2}}$, which is merely a function of the Strouhal number based on the outer variables:

$$\delta_A^+/(Rc_f)^{\frac{1}{2}} = 2(\overline{w}^s/2\omega r_i)^{\frac{1}{2}}. \tag{29}$$

The experimental values of Z_τ were obtained at values of $\delta_A^+/(Rc_f)^{\frac{1}{2}}$ ranging from 0·1 to 0·8; thus coincidence with the bursting frequency occurred within this range but δ_A^+ was well below δ_{AC}^+, in most cases. The majority of the data were measured by the sound propagation method (§2). There are not, however, enough data to allow the necessary extrapolation to zero Mach number at fixed values of δ_A^+ as well as of R. In order still to answer the question of whether or not the outer variables affect the wall shear stress impedance even at low values of δ_A^+/δ_{AC}^+, the extrapolation to $M = 0$ was conducted separately for the three pipes investigated here. The result is plotted on figure 14. On the average, the Reynolds number associated with the data points at a definite δ_A^+ increases in proportion to the pipe diameter but, on the other hand, possible effects of the outer variables are extrapolated to low Reynolds numbers since the Mach number and the Reynolds number are proportional at a fixed pipe diameter. So definite Reynolds numbers cannot be assigned to the data points of figure 14 except by further assumptions about the possible effect of the outer variables on the wall shear stress impedance. A rough estimation of the relation between

the outer and the inner Strouhal number in the case of the extrapolated wall shear stress impedance was based on the conjecture that the effect under consideration depends logarithmically on the outer Strouhal number. The dashed curves on figure 15 depict the result of this estimation and the solid curve represents the data which were obtained in the resonator experiment (§3). So a reasonable range of outer Strouhal numbers has been covered by the experiments [equation (29)]. However, the data points on figure 14 do not exhibit very significant differences between the three pipes for the sound propagation experiment nor between the results of two experiments which were conducted at rather different outer Strouhal numbers, according to figure 15. Only the data obtained in the narrowest pipe ($2r_i = 13$ mm) seem to depart a little from the rest of the data, but it is not clear whether the measurement accuracy was sufficient in this case since the sound wavenumber was measured at only three different frequencies in the 13 mm pipe.

Thus one may conclude that the wall shear stress impedance depends, at most, rather weakly on the outer variables of the turbulent boundary layer for the small values of δ_A^+/δ_{AC}^+ investigated here. This implies that the coincidence between the frequency of the shear wave and the bursting frequency has no noticeable effect on the wall impedance of the shear wave.

4.4. *Wall shear stress impedance in drag-reducing flow*

As outlined in §4.2, $Z_\tau(\delta_A^+)$ contains information about the dynamic properties of the turbulence close to the wall. Even if it is not possible to obtain all the information which is needed to determine, for example, the hypothetical viscoelasticity of the turbulence as a function of the distance from the wall, it appears to be interesting to use this method to investigate the turbulence of drag-reducing flow of dilute solutions of high polymers. From the phenomenon of drag reduction it is obvious that only a little tuning of the right 'knob' of the system turbulence is needed to modify greatly the equilibrium of this system. It seems that the viscoelasticity of the high polymer molecules plays a predominant role in this phenomenon (Bark, Hinch & Landahl 1975), and that the turbulence close to the wall is especially affected by the additives.

Thus the wall shear stress impedance was measured in an aqueous 20 p.p.m. Separan solution which exhibited a drag reduction of 40 % at low shear stresses and 25 % at high shear stresses in agreement with measurements made by Whitsitt, Harrington & Crawford (1969). The measured values of $Z_\tau(\delta_A^+)$ obtained by the resonator pipe method are plotted on figure 16. The uncertainty of the data is much higher than in the case of pure water. To some extent, this is caused by the occurrence of higher flow velocities for the same values of δ_A^+ in the case of drag reduction. In spite of the large scatter in the data, one is able to realize that the real part of Z_τ is practically unaffected by the turbulence at $\delta_A^+ < 11$; for $\delta_A^+ > 11$ up to the maximum attainable δ_A^+, Re Z_τ is smaller than unity. By way of contrast, Z_τ departs from $1+i$ at $\delta_A^+ > 8$ in Newtonian fluids. So the onset of influence of the interaction between the turbulence and the shear wave on the wall shear stress impedance is shifted to higher values of δ_A^+ in drag-reducing fluids. This corresponds to the thickening of the viscous sublayer in the high polymer solution; at $\delta_A^+ = 11$ a drag reduction of 25 % is observed, which indicates that the thickness of the sublayer has been enlarged by a factor of 1·33 relative to that for Newtonian fluids. Thus, in fact, the onset of the response of the wall shear stress impedance to the turbulence should be shifted from

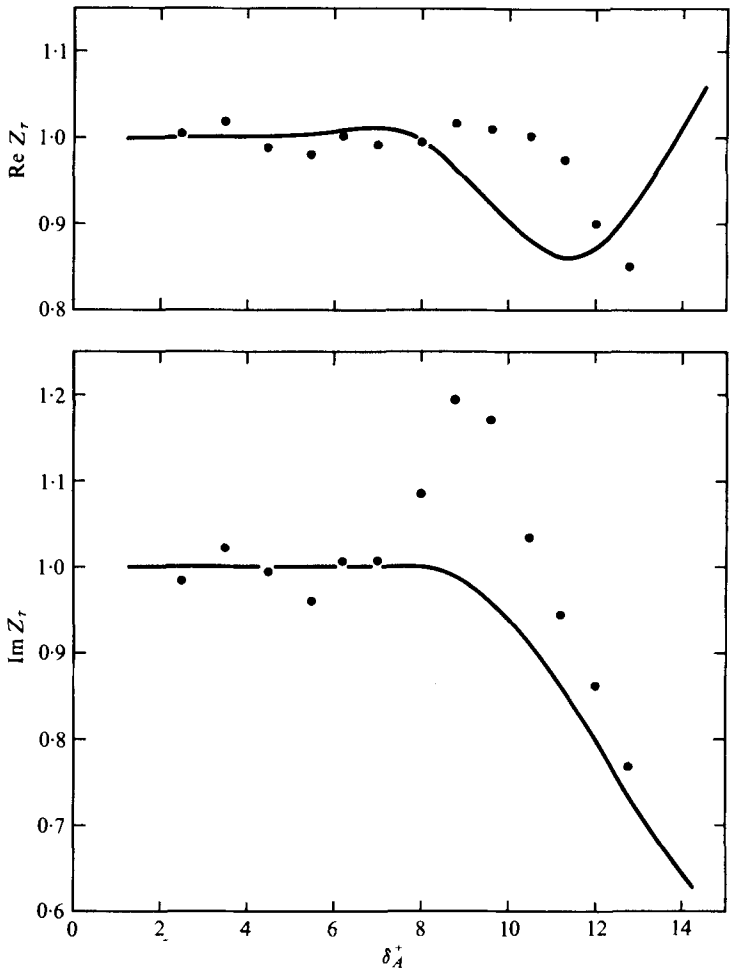

FIGURE 16. Normalized wall shear stress impedance in a 20 p.p.m. aqueous Separan solution; for comparison, the solid curves depict the result obtained in Newtonian fluids.

$\delta_A^+ = 8$ to $\delta_A^+ = 10{\cdot}7$, if all other relations remain unchanged. At present, the maximum value of δ_A^+ attainable in our experimental device is too small to allow any further statements about the wall shear stress impedance in drag-reducing flow, but measurements in a more suitable device are being prepared. The present device has some fundamental disadvantages with respect to the investigation of non-Newtonian fluids: δ_A^+ is varied by variation of the flow velocity; this means, however, that the characteristics of the non-Newtonian fluid flow (e.g. the drag reduction) are varied simultaneously. Furthermore, the high friction velocity needed for sufficiently large values of δ_A^+ in the resonator pipe causes degradation of the high polymer additives.

5. Conclusions

Small amplitude sinusoidal shear waves have been excited at the wall of a pipe carrying fully developed turbulent flow. The waves are polarized in the flow direction

and propagate into the turbulent medium, from which they are partly reflected. So information on the stress-to-strain ratio associated with this definite coherent perturbation of the turbulent flow is transported to the wall and can be extracted from the wall impedance of the shear wave. This impedance is the complex ratio of shear stress to velocity in the shear wave evaluated at the wall.

When the shear wave decays within the inner portion of the turbulent boundary layer, the wall shear stress impedance essentially depends only on the Strouhal number based on inner variables. So the coupling between the inner and the outer layer revealed by the bursting phenomenon does not significantly influence the dynamics of the turbulent shear stress within the inner layer at the low Strouhal numbers (high δ_A^+) at which the wall shear stress impedance is affected by turbulent stresses. The general trend of the impedance as a function of the inner Strouhal number can be understood by simple geometric considerations: the shear wave is reflected from the edge of the viscous sublayer. The interference between the incident and the reflected wave becomes obvious through a minimum of the real part of the impedance. However, the minimum is even deeper than that predicted by a model which replaces the edge of the viscous sublayer by a rigid plate. This fact probably demonstrates a quasi-elastic behaviour of the turbulent medium for reasons which are outlined in §4.2.

However the question of whether the turbulent stress in the shear wave can be described by a local effective viscoelasticity of the turbulent medium cannot be answered by the present investigation. Two simple models based on eddy viscosity and eddy viscoelasticity, respectively, failed completely. The minimum of the real part of the wall shear stress impedance is practically absent in the curves which are computed on the basis of these models. This indicates that the hypothetical effective viscosity either must be negative or must exhibit rather abrupt changes at the edge of the viscous sublayer. So it is rather unlikely that the shear stresses in the shear wave can be described by a local constitutive law of the turbulence.

The shear stresses in the shear wave, as a function of the distance from the wall, cannot be evaluated explicitly from the wall shear stress impedance, and further experiments are necessary. Karlsson (1958), as well as Acharya & Reynolds (1975), has measured the oscillating component $\tilde{u}$ of the streamwise velocity in a turbulent wall boundary layer with a small amplitude oscillating pressure gradient superimposed in the streamwise direction. As in our sound propagation experiment, the oscillating velocity field is then composed of a plug flow and a shear wave excited at the wall. In principle, the oscillating shear stress can be calculated from the velocity field; however Acharya & Reynolds did not obtain reliable results on doing so. The failure of their trial is probably caused by the fact that the tail of the shear wave is buried in the plug flow and cannot be extracted from the measured data with sufficient accuracy. So the experimental investigation of a pure shear wave excited by oscillations of the wall is more promising with respect to the evaluation of the oscillating shear stress. Such an experiment is being conducted in Göttingen at present.

Last but not least, some progress in computing the sound propagation in low Mach number turbulent boundary layers has been achieved by the present investigation. However, in many cases of practical interest, the Mach number is not small and

the convective term in the momentum equation affects the propagation of the shear wave. So somewhat deeper insight into the dynamics of the Reynolds stresses may possibly be obtained by comparing the sound wavenumber measured at moderate Mach numbers (§2) with values predicted on the basis of the stress-to-strain ratio measured in a shear wave exhibiting no variation in the streamwise direction (absence of convective terms). Information on how the stress-to-strain ratio depends on the form of the coherent perturbation may be yielded by this procedure.

The experiments with the oscillating pipe were sponsored by the Procurement Executive, Ministry of Defence, London. One of the authors (D.R.) is also indebted to the Deutsche Forschungsgemeinschaft, which supported the work connected with the experiment described in §2. The rather extended numerical calculations were performed on a Honeywell H 632 computer which was funded by the Stiftung Volkswagenwerk.

Appendix

Calculation of the wave propagation in a tube containing a fluid

It is assumed that the wavelength is large compared with the diameter of the tube. Then one obtains for the tube

$$\rho_t \frac{\partial \tilde{u}_t}{\partial_t} + \frac{\partial \tilde{p}_t}{\partial x} + \frac{2r_i^2}{r_o^2 - r_i^2} z_\tau (\tilde{u}_t - \tilde{u}_w) = 0, \tag{A 1}$$

$$\frac{\partial \tilde{u}_t}{\partial x} + \frac{1}{E}\left(\frac{\partial \tilde{p}_t}{\partial t} + \frac{2}{m}\frac{r_i^2}{r_o^2 - r_i^2}\frac{\partial \tilde{p}_w}{\partial t}\right) = 0 \tag{A 2}$$

and for the fluid

$$\rho_w \frac{\partial \tilde{u}_w}{\partial t} + \frac{\partial \tilde{p}_w}{\partial x} + \frac{2}{r_i} z_\tau (\tilde{u}_w - \tilde{u}_t) = 0, \tag{A 3}$$

$$\frac{\partial \tilde{u}_w}{\partial x} + \frac{2}{E}\left[\left(\frac{r_o^2 + r_i^2}{r_o^2 - r_i^2} + \frac{1}{m}\right)\frac{\partial \tilde{p}_w}{\partial t} + \frac{1}{m}\frac{\partial \tilde{p}_t}{\partial t}\right] + \frac{1}{\rho_w c_w^2}\frac{\partial \tilde{p}_w}{\partial t} = 0. \tag{A 4}$$

Here the subscripts t and w refer to the tube and to the fluid, respectively, $-\tilde{p}_t$ is the tension stress in the axial direction, $\tilde{u}_w$ is the oscillatory velocity of the fluid averaged over the cross-section and E and m^{-1} are the Young's modulus and Poisson number of the tube material. Equations (A 1) and (A 3) are based on the conservation of momentum and (A 2) and (A 4) reflect the conservation of matter, regarding the deformation of a tube exposed to tension stress and to internal pressure. Introducing the wave factor $\exp[i(\omega t - kx)]$ and the sound velocity $c_t = (E/\rho_t)^{\frac{1}{2}}$ for the empty tube yields

$$\begin{pmatrix} k & -\omega\rho_t + iz_\tau \dfrac{2r_i}{r_o^2 - r_i^2} & 0 & -iz_\tau \dfrac{2r_i}{r_o^2 - r_i^2} \\ -\dfrac{\omega}{\rho_t c_t^2} & k & -\dfrac{2\omega}{m\rho_t c_t^2}\dfrac{r_i^2}{r_o^2 - r_i^2} & 0 \\ 0 & -iz_\tau \dfrac{2}{r_i} & k & -\omega\rho_w + iz_\tau \dfrac{2}{r_i} \\ -\dfrac{2\omega}{m\rho_t c_t^2} & 0 & -\omega\left[\dfrac{2}{\rho_t c_t^2}\left(\dfrac{r_o^2 + r_i^2}{r_o^2 - r_i^2} + \dfrac{1}{m}\right) + \dfrac{1}{\rho_w c_w^2}\right] & k \end{pmatrix} \begin{pmatrix} \tilde{p}_t \\ \tilde{u}_t \\ \tilde{p}_w \\ \tilde{u}_w \end{pmatrix} = 0. \tag{A 5}$$

To begin with (A 5) is solved for $z_\tau = 0$. Essentially, two different solutions are obtained, corresponding to waves which propagate mainly in the tube or in the fluid, respectively: (*a*) the tube wave

$$\left.\begin{aligned}
\left(\frac{k_t}{\omega/c_t}\right)^2 &= \frac{\rho_w}{\rho_t}\left(\frac{r_o^2+r_i^2}{r_o^2-r_i^2}+\frac{1}{m}\right)+\frac{1}{2}\left(\left(\frac{c_t}{c_w}\right)^2+1\right) \\
&\quad -\left\{\left[\frac{\rho_w}{\rho_t}\left(\frac{r_o^2+r_i^2}{r_o^2-r_i^2}+\frac{1}{m}\right)+\frac{1}{2}\left(\left(\frac{c_t}{c_w}\right)^2-1\right)\right]^2+\frac{4}{m^2}\frac{\rho_w}{\rho_t}\frac{r_i^2}{r_o^2-r_i^2}\right\}^{\frac{1}{2}} = \left(\frac{c_t}{c_t'}\right)^2 \\
&\approx 1-\frac{\dfrac{4}{m^2}\dfrac{\rho_w}{\rho_t}\dfrac{r_i^2}{r_o^2-r_i^2}}{\left(\dfrac{c_t}{c_w}\right)^2-1+2\dfrac{\rho_w}{\rho_t}\left(\dfrac{r_o^2+r_i^2}{r_o^2-r_i^2}+\dfrac{1}{m}\right)}, \\
\tilde{u}_{tt}/\tilde{p}_{tt} &= 1/\rho_t c_t', \quad \tilde{u}_{wt}/\tilde{p}_{wt} = 1/\rho_w c_t', \\
\frac{\tilde{p}_{wt}}{\tilde{p}_{tt}} &\approx -\frac{2}{m}\frac{\rho_w}{\rho_t}\left[\left(\frac{c_t}{c_w}\right)^2-1+2\frac{\rho_w}{\rho_t}\left(\frac{r_o^2+r_i^2}{r_o^2-r_i^2}+\frac{1}{m}\right)\right]^{-1};
\end{aligned}\right\} \tag{A 6a}$$

(*b*) the fluid wave

$$\left.\begin{aligned}
\left(\frac{k_w}{\omega/c_w}\right)^2 &= \frac{\rho_w c_w^2}{\rho_t c_t^2}\left(\frac{r_o^2+r_i^2}{r_o^2-r_i^2}+\frac{1}{m}\right)+\frac{1}{2}\left(1+\left(\frac{c_w}{c_t}\right)^2\right) \\
&\quad +\left\{\left[\frac{\rho_w c_w^2}{\rho_t c_t^2}\left(\frac{r_o^2+r_i^2}{r_o^2-r_i^2}+\frac{1}{m}\right)+\frac{1}{2}\left(1-\left(\frac{c_w}{c_t}\right)^2\right)\right]^2+\frac{4}{m^2}\frac{\rho_w c_w^4}{\rho_t c_t^4}\frac{r_i^2}{r_o^2-r_i^2}\right\}^{\frac{1}{2}} = \left(\frac{c_w}{c_w'}\right)^2 \\
&\approx 1+2\frac{\rho_w c_w^2}{\rho_t c_t^2}\left[\frac{r_o^2+r_i^2}{r_o^2-r_i^2}+\frac{1}{m}+\frac{\dfrac{2}{m^2}\dfrac{r_i^2}{r_o^2-r_i^2}}{\left(\dfrac{c_t}{c_w}\right)^2-1+2\dfrac{\rho_w}{\rho_t}\left(\dfrac{r_o^2+r_i^2}{r_o^2+r_i^2}+\dfrac{1}{m}\right)}\right], \\
\tilde{u}_{ww}/\tilde{p}_{ww} &= 1/\rho_w c_w', \quad \tilde{u}_{tw}/\tilde{p}_{tw} = 1/\rho_t c_w', \\
\frac{\tilde{p}_{tw}}{\tilde{p}_{ww}} &\approx \frac{2}{m}\frac{r_i^2}{r_o^2-r_i^2}\left[\left(\frac{c_t}{c_w}\right)^2-1+2\frac{\rho_w}{\rho_t}\left(\frac{r_o^2+r_i^2}{r_o^2-r_i^2}+\frac{1}{m}\right)\right]^{-1}.
\end{aligned}\right\} \tag{A 6b}$$

Since $|z_\tau| \ll r_i\omega\rho_w$, the full solution of (A 5) is obtained by a perturbation calculation. In addition, it turns out that only the wavenumber accurate to linear terms of z_τ is needed in the next subsection. Introducing

$$k_t^2 = (\omega/c_t')^2+\delta(k_t^2), \quad k_w^2 = (\omega/c_w')^2+\delta(k_w^2)$$

yields

$$\frac{\delta(k_t^2)}{(\omega/c_t')^2} = -2\frac{iz_\tau}{\omega\rho_t}\frac{r_i}{r_o^2-r_i^2}\frac{\left(\dfrac{c_t}{c_w}\right)^2-1+\dfrac{4}{m}+2\dfrac{\rho_w}{\rho_t}\left(\dfrac{r_o^2+r_i^2}{r_o^2-r_i^2}+\dfrac{1}{m}\right)}{\left(\dfrac{c_t}{c_w}\right)^2-1+2\dfrac{\rho_w}{\rho_t}\left(\dfrac{r_o^2+r_i^2}{r_o^2-r_i^2}+\dfrac{1}{m}-\dfrac{2}{m^2}\dfrac{r_i^2}{r_o^2-r_i^2}\right)},$$

$$\frac{\delta(k_w^2)}{(\omega/c_w')^2} \approx -2\frac{iz_\tau}{\omega\rho_w r_i}\frac{1+2\dfrac{\rho_w c_w^2}{\rho_t c_t^2}\left(\dfrac{r_o^2+r_i^2}{r_o^2-r_i^2}+\dfrac{1}{m}-\dfrac{2}{m}\dfrac{r_i^2}{r_o^2-r_i^2}\right)-\left(\dfrac{c_w}{c_t}\right)^2}{1-\left(\dfrac{c_w}{c_t}\right)^2\left[1-2\dfrac{\rho_w c_w^2}{\rho_t c_t^2}\left(\dfrac{r_o^2+r_i^2}{r_o^2-r_i^2}+\dfrac{1}{m}+\dfrac{4}{m^2}\dfrac{r_i^2}{r_o^2-r_i^2}\right)\right]}.$$

Calculation of the complex resonance frequency of the resonator described in § 3.2

The resonator is excited by a thin ring of PZT (see figure 6). The excitation is most efficient when the load, i.e. the mechanical impedance of the end of the resonator, is a minimum. Because of the high quality factor of the resonance considered here, it is reasonable to assume that other possible resonances of the complex structure of the resonator are either so broad or so far away that they do not influence the resonance curve, which is expressed in terms of the input impedance of the resonator:

$$Z_r = \tilde{p}_r/\tilde{u}_r = iC'(\omega-\Omega). \tag{A 7}$$

C' can be regarded as constant within a narrow range of frequencies around the resonance. Indeed, it turns out that experimental values agree very well with (A 7). Furthermore, the changes in the complex resonance frequency caused by the actions of the wall shear stress impedance z_r and the sound radiation into the flow system are additive if these actions themselves do not exhibit strong dependence on the frequency. For this reason and because the imaginary part of Ω is very small compared with the real part, the change in Ω can be calculated assuming Ω_o to be real (Ω_o is the resonance frequency for $z_r = 0$ and for $L_{wa} = L_{wb} = 0$, where $L_{wa} = [-\tilde{u}_w/\tilde{p}_w]_{x=-l}$ and $L_{wb} = [\tilde{u}_w/\tilde{p}_w]_{x=l}$ are the water sound admittances at the ends of the central pipe carrying the turbulent flow). Also it is assumed that

$$L_{tb} = i(\omega-\Omega_o)\, l_{\text{end}}/\rho_t c_t'^2, \tag{A 8}$$

where $L_{tb} = [\tilde{u}_t/\tilde{p}_t]_{x=l}$ and l_{end} is the effective length of the end pieces of the resonator (this assumption is equivalent to $l\Omega_o/c_t' = \frac{1}{2}\pi$). Decomposition of the pressures and of the velocities into four waves yields

$$L_{wa} = -\frac{\tilde{u}_{ww1}\exp(ik_w l)-\tilde{u}_{ww2}\exp(-ik_w l)+\tilde{u}_{wt1}\exp(ik_t l)-\tilde{u}_{wt2}\exp(-ik_t l)}{\tilde{p}_{ww1}\exp(ik_w l)+\tilde{p}_{ww2}\exp(-ik_w l)+\tilde{p}_{wt1}\exp(ik_t l)+\tilde{p}_{wt2}\exp(-ik_t l)}, \tag{A 9a}$$

$$L_{wb} = \frac{\tilde{u}_{ww1}\exp(-ik_w l)-\tilde{u}_{ww2}\exp(ik_w l)+\tilde{u}_{wt1}\exp(-ik_t l)-\tilde{u}_{wt2}\exp(ik_t l)}{\tilde{p}_{ww1}\exp(-ik_w l)+\tilde{p}_{ww2}\exp(ik_w l)+\tilde{p}_{wt1}\exp(-ik_t l)+\tilde{p}_{wt2}\exp(ik_t l)}, \tag{A 9b}$$

and analogous relations for L_{tb} and $L_{ta} = [\tilde{u}_t/\tilde{p}_t]_{x=-l}$, where the indices 1 and 2 stand for waves propagating in the $\pm$ x directions respectively. Approximating $\exp(\pm ik_t l)$ by $\pm i(1+\delta k_t l)$ and solving (A9) for L_{ta} yields

$$L_{ta} \approx \frac{2i\delta k_t l}{\rho_t c_t'} + i\frac{(\omega-\Omega_o)\, l_{\text{end}}}{\rho_t c_t'^2} + \frac{\dfrac{8}{m^2}\dfrac{\rho_w}{\rho_t}\dfrac{r_i^2}{r_o^2-r_i^2}\dfrac{1}{\rho_t c_w'}}{\left[\left(\dfrac{c_t}{c_w}\right)^2 - 1 + 2\dfrac{\rho_w}{\rho_t}\left(\dfrac{r_o^2+r_i^2}{r_o^2-r_i^2}+\dfrac{1}{m}\right)\right]^2} \frac{1+iw\tan k_w l-2\delta_L^2}{(w+i\tan k_w l)(1+iw\tan k_w l)-2i\delta_L^2\tan k_w l}, \tag{A 10}$$

where $\delta k_t = \delta(k_t^2)/(2\omega/c_t')$, $w = 2\rho_w c_w'/(L_{wb}+L_{wa})$ and $\delta_L = (L_{wb}-L_{wa})/(L_{wb}+L_{wa})$. Finally, one obtains by transformation of L_{ta} into the input impedance Z_r of the resonator and by comparison with (A 7)

$$\delta\Omega = \Omega-\Omega_o \approx \frac{ic_t'}{2(l+l_{\text{end}})}\left[2i\delta k_t l + \frac{\frac{8}{m^2}\frac{\rho_w}{\rho_t}\frac{r_i^2}{r_o^2-r_i^2}\frac{c_t'}{c_w'}}{\left[\left(\frac{c_t}{c_w}\right)^2-1+2\frac{\rho_w}{\rho_t}\left(\frac{r_o^2+r_i^2}{r_o^2-r_i^2}+\frac{1}{m}\right)\right]^2}\frac{1+iw\tan k_w l-2\delta_L^2}{(w+i\tan k_w l)(1+iw\tan k_w l)-2i\delta_L^2\tan k_w l}\right]. \tag{A 11}$$

REFERENCES

ACHARYA, M. & REYNOLDS, W. C. 1975 Measurements and predictions of a fully developed turbulent channel flow with imposed controlled oscillations. *Dept. Mech. Engng, Stanford Univ. Rep.* TF-8.

AHRENS, C. 1973 Wechselwirkung zwischen Zähigkeitswellen und wandnaher Turbulenz in Wasser mit und ohne Zusatz einer reibungsvermindernden Substanz. Ph.D. dissertation, Math.-Nat. Fakultät Universität Göttingen.

AHRENS, C. & RONNEBERGER, D. 1971 Luftschalldämpfung in turbulent durchströmten, schallharten Rohren bei verschiedenen Wandrauhigkeiten. *Acustica* **25**, 150.

BARK, F. H., HINCH, E. J. & LANDAHL, M. T. 1975 Drag reduction in turbulent flow due to additives: a report on Euromech 52. *J. Fluid Mech.* **68**, 129.

BROCHER, E. 1977 Oscillatory flows in ducts: a report on Euromech 73. *J. Fluid Mech.* **79**, 113.

CEBECI, T. 1973 A model for eddy conductivity and turbulent Prandtl number. *J. Heat Transfer* **95**, 227.

DAVIS, R. E. 1972 On prediction of the turbulent flow over a wavy boundary. *J. Fluid Mech.* **52**, 287.

DAVIS, R. E. 1974 Perturbed turbulent flow, eddy viscosity and the generation of turbulent stresses. *J. Fluid Mech.* **63**, 673.

DRIEST, E. R. VAN 1956 On turbulent flow near a wall. *J. Aero. Sci.* **23**, 1007.

ECKELMANN, H. 1970 Experimentelle Untersuchungen in einer turbulenten Kanalströmung mit starken viskosen Wandschichten. *Mitt. MPI Strömungsforsch. AVA Göttingen* no. 48.

EICHELBRENNER, E. A. (ed.) 1971 *Recent Research on Unsteady Boundary Layers. IUTAM Symp.* Laval University Press.

HUSSAIN, A. K. M. F. & REYNOLDS, W. C. 1970*a* The mechanics of a perturbation wave in turbulent shear flow. *Dept. Mech. Engng Stanford Univ. Rep.* FM-6.

HUSSAIN, A. K. M. F. & REYNOLDS, W. C. 1970*b* The mechanics of an organized wave in turbulent shear flow. *J. Fluid Mech.* **41**, 241.

HUSSAIN, A. K. M. F. & REYNOLDS, W. C. 1972 The mechanics of an organized wave in turbulent shear flow. Part 2. Experimental results. *J. Fluid Mech.* **54**, 241.

KARLSSON, S. K. F. 1958 An unsteady turbulent boundary layer. *J. Fluid Mech.* **5**, 622.

KENDALL, J. M. 1970 The turbulent boundary layer over a wall with progressive surface waves. *J. Fluid Mech.* **14**, 385.

KLINE, S. J., REYNOLDS, W. C., SCHRAUB, F. A. & RUNSTADLER, P. W. 1967 The structure of turbulent boundary layers. *J. Fluid Mech.* **30**, 741.

LANDAHL, M. T. 1967 A wave guide model for turbulent shear flow. *J. Fluid Mech.* **29**, 441.

LAUFER, J. & BADRI NARAYANAN, M. A. 1971 Mean period of the turbulent production mechanism in a boundary layer. *Phys. Fluids* **14**, 182.

LUDWIEG, H. 1956 Bestimmung des Verhältnisses der Austauschkoeffizienten für Wärme und Impuls bei turbulenten Grenzschichten. *Z. Flugwiss.* **4**, 73.

NORRIS, H. L. & REYNOLDS, W. C. 1975 Turbulent channel flow with a moving wavy boundary. *Dept. Mech. Engng, Stanford Univ. Rep.* TF-7.

RAO, K. N., NARASIMHA, R. & BADRI NARAYANAN, M. A. 1971 The 'bursting' phenomenon in a turbulent boundary layer. *J. Fluid Mech.* **48**, 339.

REICHARDT, H. 1951 Vollständige Darstellung der turbulenten Geschwindigkeitsverteilung in glatten Leitungen. *Z. angew. Math. Mech.* **31**, 208.

REYNOLDS, W. C. & HUSSAIN, A. K. M. F. 1972 The mechanics of an organized wave in turbulent shear flow. Part 3. Theoretical models and comparisons with experiments. *J. Fluid Mech.* **54**, 263.

RONNEBERGER, D. 1975 Genaue Messung der Schalldämpfung und der Phasengeschwindigkeit in durchströmten Rohren im Hinblick auf die Wechselwirkung zwischen Schall und Turbulenz. *Habilitationsschrift Math. Nat. Fak. Univ.* Göttingen.

STEWART, R. H. 1970 Laboratory studies of the velocity field of deep-water waves. *J. Fluid Mech.* **42**, 733.

VASILIEV, O. F. & KVON, V. I. 1971 Unsteady turbulent shear flow in a pipe. In *Recent Research on Unsteady Boundary Layers. IUTAM Symp.* (ed. E. A. Eichelbrenner), p. 2028. Laval University Press.

WHITSITT, N. F., HARRINGTON, L. J. & CRAWFORD, H. R. 1969 Effect of wall shear stress on drag reduction of viscoelastic solutions. In *Viscous Drag Reduction* (ed. C. S. Wells), p. 265.